



Pavels Dimitrijevs

# Targeting Cancer Metabolism with Isoselenazolium Salts

Summary of the Doctoral Thesis for obtaining  
the scientific degree “Doctor of Science (*PhD*)”

Sector Group – Medicine and Health Sciences

Sector – Basic Medicine

Sub-Sector – Pharmaceutical Pharmacology

Rīga, 2023



Pavels Dimitrijevs

ORCID 0000-0002-6332-2395

## Targeting Cancer Metabolism with Isoselenazolium Salts

Summary of the Doctoral Thesis for obtaining  
the scientific degree “Doctor of Science (*PhD*)”

Sector Group – Medicine and Health Sciences

Sector – Basic Medicine

Sub-Sector – Pharmaceutical Pharmacology

Riga, 2023

The Doctoral Thesis was developed at Latvian Institute of Organic Synthesis

Supervisor of the Doctoral Thesis:

*Dr. chem.*, LAS full member **Pavels Arsenjans**,  
Latvian Institute of Organic Synthesis

Official Reviewers:

*Dr. pharm.*, Professor **Dace Bandere**,  
Rīga Stradiņš University. Latvia

*Dr. med. sci.*, Professor **Una Riekstiņa**,  
University of Latvia

*Dr. med. sci.*, Professor **Ago Rinken**,  
University of Tartu, Estonia

Defence of the Doctoral Thesis will take place at the public session of the Promotion Council of Basic Medicine on 15 January 2024 at 14.00 in the Hippocrates Lecture Theatre, 16 Dzirciema Street, Rīga Stradiņš University and remotely via online platform *Zoom*

The Doctoral Thesis is available in RSU Library and on RSU website: <https://www.rsu.lv/en/dissertations>

NATIONAL  
DEVELOPMENT  
PLAN 2020



EUROPEAN UNION  
European Regional  
Development Fund

INVESTING IN YOUR FUTURE

This work was supported by ERDF “Development of a novel potent PARP inhibitor” (No. 1.1.1.1/19/A/016) and BioMedPharm (No. VPP-EM-BIOMEDICINA-2022/1-0001) projects.

Secretary of the Promotion Council:

*Dr. chem.*, Associate Professor **Māra Plotniece**

# Table of Contents

Abbreviations used in the Thesis .....	4
Introduction .....	7
Aim of the Thesis .....	8
Tasks of the Thesis .....	8
Hypotheses of the Thesis .....	9
Novelty of the Thesis .....	9
1 Results .....	10
1.1 Effects of isoselenazolium salts on cancer metabolism .....	10
1.1.1 Isoselenazolium salts cytotoxicity .....	10
1.1.2 Modulation of mitochondrial respiration and ROS production .....	12
1.1.3 Impact on NAD <sup>+</sup> homeostasis .....	15
1.1.4 Poly(ADP-ribose)polymerase 1 inhibitory activity .....	16
1.1.5 Interaction with cardiolipin .....	16
1.2 Development of the new cardiolipin-specific fluorescent probe .....	18
1.2.1 Synthesis of the new cardiolipin-specific fluorescent probes .....	19
1.2.2 Cardiolipin quantitative analysis .....	23
1.2.3 Fluorescence-based competitive binding assay .....	26
1.2.4 Isoselenazolium salts affinity for cardiolipin .....	29
1.3 The second generation of isoselenazolium salts and their mechanism of action .....	29
1.3.1 Synthesis of new isoselenazolium derivatives .....	29
1.3.2 Cytotoxicity of the new isoselenazolium derivatives .....	32
1.3.3 Influence on mitochondrial respiration, ROS production and coupling state of the electron transfer system .....	34
1.3.4 Enzymatic screening of isoselenazolium salts .....	37
1.3.5 Pyruvate kinase M2 inhibition mechanisms .....	40
1.3.6 Alterations in mRNA expression of pyruvate kinases M2 and M1 .....	45
1.3.7 Prevention of pyruvate kinase M2 nuclear translocation .....	46
2 Discussion .....	50
Conclusions .....	55
List of publications, reports and patents on the topic of the Thesis .....	56
References .....	57
Acknowledgements .....	63

## Abbreviations used in the Thesis

ATP	adenosine triphosphate
ADP	adenosine diphosphate
ANOVA	analysis of variance
AO	acridine orange, 3,6-bis(dimethylamino)acridine
Bcl-2	B-cell lymphoma 2 protein
CI	respiratory complex I, NADH:ubiquinone oxidoreductase
CII	respiratory complex II, succinate dehydrogenase
CIII	respiratory complex III, coenzyme Q – cytochrome c reductase
CL	cardiolipin
Cyt c	cytochrome c
DAPI	4',6-diamidino-2-phenylindole
DCM	dichloromethane
DMF	dimethylformamide
DMSO	dimethyl sulfoxide
DNA	deoxyribonucleic acid
DOPC	1,2-dioleoyl- <i>sn</i> -glycero-3-phosphocholine
DSF	differential scanning fluorimetry
EC <sub>50</sub>	the half-maximal effective concentration
EDC	1-ethyl-3-(3-dimethylaminopropyl)carbodiimide
ESKAPE	<i>Enterococcus faecium</i> , <i>Staphylococcus aureus</i> , <i>Klebsiella pneumoniae</i> , <i>Acinetobacter baumannii</i> , <i>Pseudomonas aeruginosa</i> , and <i>Enterobacter spp.</i>
ETS	electron transfer system
FBP	fructose 1,6-bisphosphate
FI	fluorescence intensity
G	glutamate
HEPES	4-(2-hydroxyethyl)-1-piperazine ethanesulfonic acid

HOBt	1-hydroxybenzotriazole
IC <sub>50</sub>	the half-maximal inhibitory concentration
IMM	inner mitochondrial membrane
ITC	isothermal titration calorimetry
K <sub>App,M</sub>	apparent Michaelis-Menten constant
LDH	lactate dehydrogenase
LEAK	non-phosphorylating resting state of mitochondrial respiration
M	malate
MeOH	methanol
mRNA	messenger ribonucleic acid
MTT	3-(4,5-dimethylthiazol-2-yl)-2,5-diphenyltetrazolium bromide
N	NADH-generating substrates
NAD <sup>+</sup>	nicotinamide adenine dinucleotide
NADH	nicotinamide adenine dinucleotide, reduced
NADPH	nicotinamide adenine dinucleotide phosphate, reduced
NAMPT	nicotinamide phosphoribosyltransferase
NAO	10- <i>N</i> -nonyl acridine orange
NMN	nicotinamide mononucleotide
NMR	nuclear magnetic resonance
NS	NADH and succinate generating substrates
OCR	oxygen consumption rate
OXPHOS	oxidative phosphorylation
P	pyruvate
PA	L- $\alpha$ -phosphatidic acid
PAr	poly(ADP-ribose)
PARP	poly(ADP-ribose) polymerase
PE	L- $\alpha$ -phosphatidylethanolamine

PEP	phosphoenolpyruvate
PI	L- $\alpha$ -phosphatidylinositol
PKM1	pyruvate kinase isoform M1
PKM2	pyruvate kinase isoform M2
PKR	pyruvate kinase isoform R
PS	L- $\alpha$ -phosphatidylserine
qPCR	quantitative polymerase chain reaction
ROS	reactive oxygen species
rot	rotenone
S	succinate
SAR	structure-activity relationship
SD	standard deviation
SEC	size exclusion chromatography
STAT3	signal transducer and activator of transcription 3
TPP	triphenylphosphonium radical
Tris	tris(hydroxymethyl)aminomethane
TTAPE-Me	1,1,2,2-tetrakis[4-(2-trimethylammonioethoxy)-phenylethene
V <sub>App,max</sub>	apparent maximum reaction velocity
V <sub>0</sub>	initial reaction velocity
Water-LOGSY	Water-ligand observed via gradient spectroscopy
$\Phi$	photoluminescence quantum yield

## Introduction

Cancer is a group of diseases caused by the accumulation of genetic mutations and dysregulated gene expression leading to uncontrolled proliferation of cells. To support growth, cancer cells must meet a high energy demand, produce building blocks for biomass generation and maintain a reduction-oxidation balance. This is achieved through so called metabolic reprogramming, which includes upregulation of glucose transport and key glycolytic enzymes, promoting aerobic glycolysis (Upadhyay et al., 2013). In addition, mitochondrial metabolism is equally important for adenosine triphosphate (ATP) production, regulation of apoptosis and tumorigenesis (Zu and Guppy, 2004; Weinberg et al., 2010; Fan et al., 2013; Weinberg and Chandel, 2015). Cancer cells maintain higher levels of reactive oxygen species (ROS) than normal cells, but despite increased antioxidant capacity, are more vulnerable to the additional ROS induction (Gorrini, Harris and Mak, 2013).

With the discovery of the fundamental roles of selenium and selenoproteins in metabolism and antioxidant systems, as well as the progress in the field of organoselenium chemistry, an intensive development of new organic Se-containing therapeutics has begun (Gandin et al., 2018). Many different classes of organoselenium compounds have been explored as anticancer agents so far, but despite promising preclinical results, none of them has yet found its place on a pharmacy shelf. The clinical application is often limited by the requirement of high doses that lead to the accumulation of toxic selenium-containing metabolites (selenosis) and serious side effects such as drug-induced liver injury, immunosuppression, anaemia and infertility (Johnson et al., 2008; Garbo et al., 2022). Another common problem with selenium-containing agents is an unclear or only superficially studied mechanism of action, which also slows down the development process of a particular class of compounds (Lenardão, Sancineto, and Santi, 2018; Chuai et al., 2021). A solution to these issues



requires a deep understanding of the mode of action, finding an objective molecular target and the development of new selenium-containing compounds with higher antiproliferative activity to reduce the effective dose and the risk of selenosis.

Recently, a new group of organoselenium compounds – fused isoselenazolium salts – has been discovered, a heterocyclic system with a Se–N<sup>+</sup> bond (Arsenyan et al., 2015). These compounds have been shown to be highly reactive pro-oxidants that induce DNA double-strand damage and display excellent antibacterial activity against ESKAPE pathogens (Arsenyan and Vasiljeva, 2017; Rendekova et al., 2017; Witek et al., 2017). However, the chemotherapeutic potential of this scaffold has not been explored yet. This Thesis describes the antiproliferative activity of isoselenazolium salts, structure-activity relationship studies, mechanism of action, challenges faced and solutions found.

## **Aim of the Thesis**

To investigate the antiproliferative activity and establish molecular mechanisms of isoselenazolium salts to increase efficacy through subsequent structural modifications.

## **Tasks of the Thesis**

In order to reach the aim of the Doctoral Thesis, the following objectives have been set:

1. Evaluate cytotoxicity of isoselenazolium salts against different malignant and normal cell lines.
2. Determine the mechanism of action of isoselenazolium salts and identify potential molecular targets.

3. Explore the structure-activity relationship of isoselenazolium derivatives based on in vitro pharmacological activity.

### **Hypotheses of the Thesis**

Substituted isoselenazolium chlorides exhibit high antiproliferative activity by targeting cancer metabolism.

### **Novelty of the Thesis**

This study provides the first extensive examination of the antiproliferative activity of isoselenazolium salts and their effect on cancer metabolism. A new fluorescence-based competitive binding assay for the determination of the binding affinity to cardiolipin was developed as part of the study, which should be of great interest to researchers working on the discovery of mitochondria-targeted drugs. The design and synthesis of the second generation of isoselenazolium derivatives led to the discovery of potent PARP1 and PKM2 inhibitors with dual activity. These findings will help in the further fundamental studies of the role of PKM2 in cancer metabolism and provide the basis for a novel class of drug candidates with a unique molecular mechanism. The novelty of the study is underlined by the two international patents for cardiolipin-specific fluorescent probes and the competitive binding assay, as well as a PCT application for the new PKM2 inhibitors.

# 1 Results

## 1.1 Effects of isoselenazolium salts on cancer metabolism

### 1.1.1 Isoselenazolium salts cytotoxicity

Cytotoxicity of fused isoselenazolium salts **1–7** (Figure 1.1) was examined against breast cancer and normal cells by MTT assay, and the results are summarised in the Table 1.1. All the compounds demonstrated higher cytotoxic activities than the reference compound,  $\text{Na}_2\text{SeO}_3$ , in breast tumour cell lines. The  $\text{IC}_{50}$  of the studied isoselenazolium salts **1–7** were similar to doxorubicin; however, mammary carcinoma (4T1) cells were generally more susceptible.

To study the influence of the fused heterocycle on the activity, the pyridine fragment was replaced with thiazole and imidazole rings obtaining thiazolo- and imidazolisoselenazolium heterocyclic systems. The introduction of the thiazole (**6**) or imidazole (**7**) rings decreased the cytotoxicity to tumour cells, however, compound **7** showed higher toxicity than compound **6** against normal cell lines. For the further research, derivatives **3**, **6** and **7** were chosen to study the possible mechanisms of action of fused isoselenazolium salts.

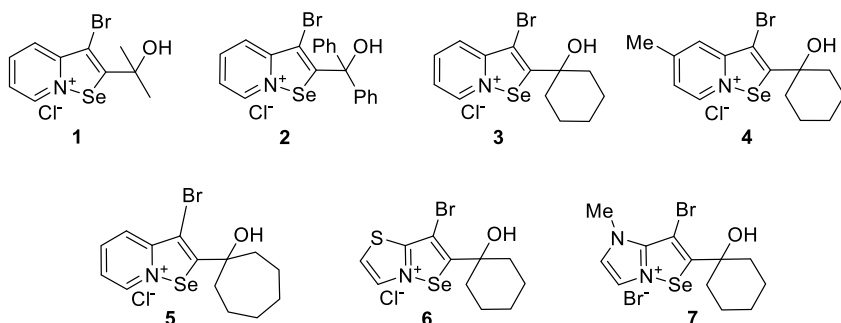


Figure 1.1 Molecular structures of fused isoselenazolium salts **1–7**

Table 1.1

## Cytotoxic activity of compounds 1–7 against breast tumour and normal cell lines

Compound	Cytotoxicity, IC <sub>50</sub> , μM							
	Breast cancer cell lines				Normal cell lines			
	MCF-7	4T1	H9C2	3T3	HEKa	MDCK	A7R5	
Na <sub>2</sub> SeO <sub>3</sub>	17.10 ± 2.40	4.90 ± 0.60	1.50 ± 0.30	22.30 ± 3.60	13.30 ± 1.10	6.30 ± 0.40	39.40 ± 8.20	
Doxorubicin	1.00 ± 0.30	0.16 ± 0.06	11.00 ± 1.00	0.75 ± 0.09	n.t.	57.00 ± 6.10	1.82 ± 0.35	
<b>1</b>	3.10 ± 0.03	0.30 ± 0.03	1.80 ± 0.10	0.13 ± 0.02	2.31 ± 0.02	3.26 ± 0.40	2.89 ± 0.42	
<b>2</b>	0.39 ± 0.03	1.10 ± 0.08	4.20 ± 0.30	1.60 ± 0.30	2.78 ± 0.08	6.27 ± 0.29	1.87 ± 0.26	
<b>3</b>	0.50 ± 0.02	0.044 ± 0.005	2.20 ± 0.10	0.39 ± 0.05	2.21 ± 0.02	2.91 ± 0.13	1.85 ± 0.22	
<b>4</b>	1.48 ± 0.04	0.45 ± 0.02	2.90 ± 0.10	0.79 ± 0.02	2.05 ± 0.05	2.54 ± 0.57	1.93 ± 0.16	
<b>5</b>	0.29 ± 0.01	0.41 ± 0.05	9.30 ± 0.20	0.98 ± 0.03	2.01 ± 0.08	1.51 ± 0.37	1.92 ± 0.44	
<b>6</b>	3.23 ± 0.03	1.70 ± 0.20	3.70 ± 0.20	7.40 ± 0.80	2.84 ± 0.08	6.58 ± 0.33	1.97 ± 0.27	
<b>7</b>	1.48 ± 0.02	0.94 ± 0.06	0.67 ± 0.02	2.20 ± 0.30	2.19 ± 0.09	4.28 ± 0.34	1.66 ± 0.25	

\*Values are shown as the means ± SD from 3 independent experiments.

n.t. – not tested.

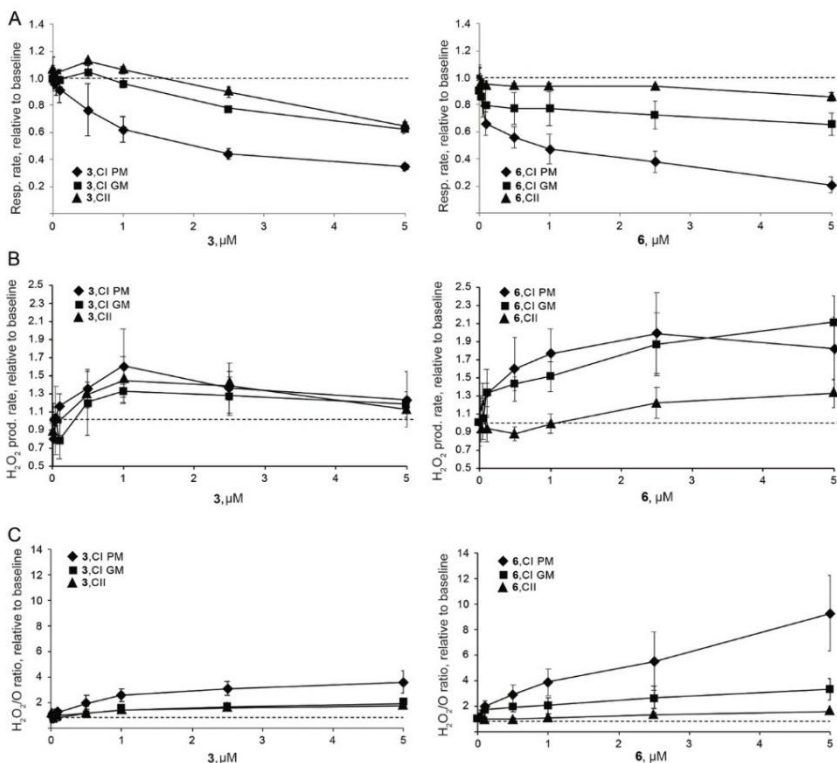
### 1.1.2 Modulation of mitochondrial respiration and ROS production

One of the most important oxidation-reduction processes in the cell are carried out in the ETS in mitochondria, which is also the main site of the intracellular ROS production. Taking in mind that isoselenazolium salts in the presence of H<sub>2</sub>O<sub>2</sub> act as a strong oxidant, it was of special interest to study their impact on mitochondrial function.

First, the concentration-dependent effects of compounds **3** and **6** on the complex I (NADH-linked) and complex II (succinate-linked) pathways were determined. Both compounds inhibited the mitochondrial respiration rate in a concentration-dependent manner and increased H<sub>2</sub>O<sub>2</sub> production with complex I (CI, NADH-linked) substrates (both pyruvate + malate and glutamate + malate) (Figure 1.2 A and B). In addition, there were no significant changes in mitochondrial function in the CII-linked OXPHOS state. Despite the difference in the compounds` potency, the most pronounced increase in the H<sub>2</sub>O<sub>2</sub>/O ratio in the presence of isoselenazolium salts **3** and **6** was observed when pyruvate and malate were used as substrates (Figure 1.2 C). These results indicated that isoselenazolium salts most likely affected pyruvate-dependent mitochondrial metabolism.

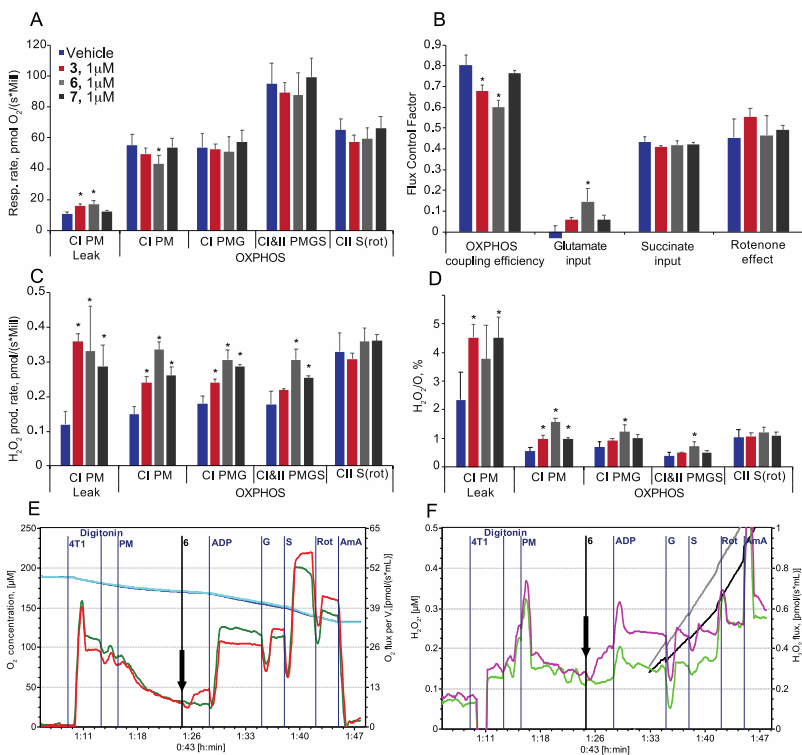
To determine whether the observed effects of the fused isoselenazolium salts were related to the inhibition of the pyruvate-dependent pathway but not to the direct inhibition of CI, the mitochondrial function in permeabilised breast cancer cells was evaluated in the presence of 1 µM of compounds **3**, **6** and **7**. Although only compound **6** decreased the respiration rate in the OXPHOS state with pyruvate and malate (Figure 1.3 A and E), both compounds **3** and **6** induced a significant decrease in the OXPHOS coupling efficiency (Figure 1.3 B). The addition of another NADH-dependent CI substrate, glutamate, compensated for the decrease in respiration with pyruvate and malate, as shown by the increased

flux control factor (characterises individual substrate/pathway input to the ET system performance) for glutamate. Together with the unchanged flux control factor for rotenone, these results indicated that fused isoselenazolium salts did not inhibit CI.



**Figure 1.2 The concentration-dependent effects of compounds 3 and 6 on mitochondrial function in permeabilised 4T1 cells. A) Concentration dependent changes in mitochondrial respiration rate; B) H<sub>2</sub>O<sub>2</sub> production rate; C) H<sub>2</sub>O<sub>2</sub>/O ratio at Complex I or II linked OXPHOS\***

\*P – pyruvate; M – malate; G – glutamate. Values are shown as mean ± SD (n = 3–5 experiments) relative to baseline (dashed line) – before addition of the compound.



**Figure 1.3 The effect of fused isoselenazolium salts 3, 6 and 7 at 1  $\mu\text{M}$  concentration on mitochondrial respiration in permeabilised 4T1 cells. A) Respiration rate; B) flux control factors; C) H<sub>2</sub>O<sub>2</sub> production rate; D) H<sub>2</sub>O<sub>2</sub>/O<sub>2</sub> ratio; E) Representative traces of respiration (green – vehicle, DMSO, red – comp. 6); F) H<sub>2</sub>O<sub>2</sub> production rate measurement (light green – vehicle, DMSO, purple – comp. 6)\***

\*CI – complex I; CII – complex II; LEAK – substrate dependent respiration rate; OXPHOS – oxidative phosphorylation dependent state; P – pyruvate; M – malate; G – glutamate; S – succinate; Rot – rotenone, AmA – antimycin A. OXPHOS coupling efficiency corresponds to  $1/\text{Respiratory control ratio}^{-1}$ . Flux control factor indicates on the input of each substrate and/or pathway to the ETS performance. Values are shown as mean  $\pm$  SD ( $n = 3-4$  experiments). Statistically significant difference (\*) was considered when  $p < 0.05$  (one-way ANOVA) compared to the control group (vehicle-DMSO).

All three tested isoselenazolium derivatives **3**, **6** and **7** induced immediate and significant increases in H<sub>2</sub>O<sub>2</sub> production and the H<sub>2</sub>O<sub>2</sub>/O ratio in the pyruvate-dependent OXPHOS state (Figure 1.3 C, D and F). The effects of compound **6** on H<sub>2</sub>O<sub>2</sub> production and the H<sub>2</sub>O<sub>2</sub>/O ratio were the most pronounced (2.3- and 2.8-fold increases, respectively). Taken together, the obtained results indicate that fused isoselenazolium salts inhibit pyruvate-dependent mitochondrial respiration and facilitate ROS production.

### 1.1.3 Impact on NAD<sup>+</sup> homeostasis

NAD<sup>+</sup> and its metabolites are used in many cellular processes and their levels are critical for tumour cell proliferation (Houtkooper et al., 2010; Poljsak, 2016; Zhu et al., 2019; Katsyuba et al., 2020).

Compounds **3** and **6** induced a decrease in NMN levels by 33 % and 26 %, respectively. In addition, compound **3** significantly decreased the levels of NAD<sup>+</sup> and NADH by 59 % and 33 %, respectively, and as a result, the NAD<sup>+</sup>/NADH ratio was decreased by 38 % (Figure 1.4 A and B). Compound **6** induced a 25 % decrease in the NAD<sup>+</sup> level without affecting the NADH content or the NAD<sup>+</sup>/NADH ratio in the cells. In contrast to compound **6**, compound **7** induced a decrease in NADH level without affecting the NAD<sup>+</sup> concentration, and as a result, increased the NAD<sup>+</sup>/NADH ratio. Notably, only imidazoloisoselenazolium salt **7** induced a moderate reduction (by 31 %) in NAMPT activity at 2 µM concentration (Figure 1.4 C).

Together, these results indicate that fused isoselenazolium salts altered NAD<sup>+</sup> homeostasis in breast tumour cells, but this impact was not exerted through the NAD<sup>+</sup> salvage pathway.



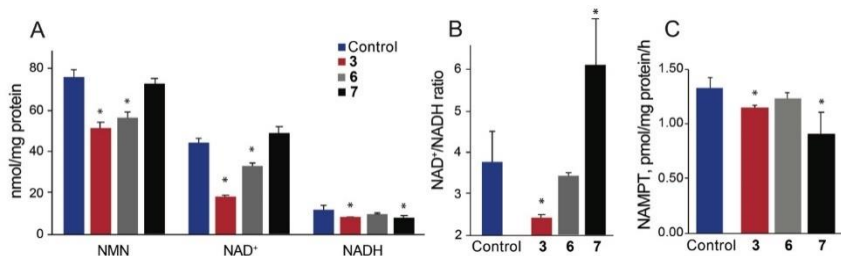


Figure 1.4 The effects of isoselenazolium salts 3,6 and 7 on the levels of NMN, NAD<sup>+</sup>, NADH and NAMPT activity in MCF-7 cells.

A) NMN, NAD<sup>+</sup> and NADH concentrations; B) NAD<sup>+</sup>/NADH ratio; C) NAMPT inhibition by 3, 6 and 7 at 2  $\mu$ M concentration\*

\*Values are shown as the mean  $\pm$  SD ( $n = 6$ ). Statistically significant difference (\*) was considered when  $p < 0.05$  (one-way ANOVA) compared to the control group (vehicle).

### 1.1.4 Poly(ADP-ribose)polymerase 1 inhibitory activity

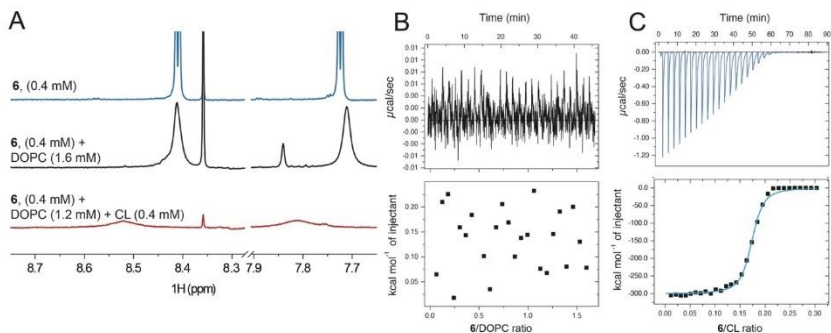
Upon excessive DNA damage PARP becomes activated and dramatically reduces NAD<sup>+</sup> levels even down to 20–30 % of their normal levels. (Houtkooper et al., 2010) Since isoselenazolium salts disturbed NAD<sup>+</sup> homeostasis, an important question was whether they modulate PARP activity. Surprisingly, it was found that compounds **3** and **7** inhibited PARP1 with IC<sub>50</sub> of  $0.970 \pm 0.030$  and  $0.880 \pm 0.010$   $\mu$ M, respectively, while compound **6** was the most active with IC<sub>50</sub>  $0.140 \pm 0.010$   $\mu$ M. Consequently, a reduction in NAD<sup>+</sup> concentration cannot be attributed to the overactivation of PARP1.

### 1.1.5 Interaction with cardiolipin

Cardiolipin (CL) is a unique phospholipid which is localised and synthesised in the inner mitochondrial membrane (IMM) where it makes up approximately 20 % of the total IMM phospholipids. It is now widely accepted that CL plays an important role in mitochondrial membrane morphology, stability, dynamics and is required for optimal activity of several mitochondrial

membrane proteins e.g. ETS complexes and cytochrome c (cyt c) (Paradies et al., 2019).

To evaluate whether fused isoselenazolium salts directly interact with CL, the interactions of derivative **6** with CL/1,2-dioleoyl-*sn*-glycero-3-phosphocholinediole (DOPC) liposomes were studied. In the absence of DOPC and CL, compound **6** showed sharp resonances with clearly distinguishable spin coupling patterns (Figure 1.5 A). In the presence of DOPC liposomes, the aromatic resonances of compound **6** were noticeably broadened such that the coupling pattern was not resolved. This could indicate a weak interaction between compound **6** and DOPC liposomes or, alternatively, the changes in resonance could be due to altered molecular surroundings (liposomal dispersion). However, in the presence of CL-containing liposomes, these resonances were significantly broadened.



**Figure 1.5 Interaction of compound 6 with CL. A) 600 MHz  $^1\text{H}$  NMR spectra of **6** (top), **6** and DOPC (middle) and **6** and DOPC with CL (bottom) in 90 %  $\text{H}_2\text{O}/10$  %  $\text{D}_2\text{O}$ , D18 HEPES, pH = 7.4 (the zoomed aromatic region is shown); B) and C) Binding isotherms and calorimetric titration curves for DOPC (B) and CL/DOPC (1:3) vesicles (C) titrations with the compound **6**.**

These results were also confirmed by the isothermal titration calorimetry (ITC) experiments (Figure 1.5 B and C). DOPC liposomes titration with compound **6** did not result in any heat release, and no signs of binding were observed. In contrast, the negative heat flow observed after each injection of compound **6** indicated that the isoselenazolium cation–CL interaction was accompanied by a decrease in enthalpy. These results indicated that compound **6** was clearly bound to the simplified mitochondrial membrane model. However, large energy release as well as broad and asymmetric peaks did not allow to estimate the precise binding affinity of compound **6**.

At that stage of the research, PARP1 and CL were identified as the most promising molecular targets for isoselenazolium salts. Screening of a larger set of compounds for PARP1 inhibitory activity can be readily done with a commercially available assay kit, however, there were no convenient and precise methods for estimating the affinity for CL. Therefore, to advance the studies of the mechanism of action, the research continued with the development of a new method for CL-targeted compound screening.

## **1.2 Development of the new cardiolipin-specific fluorescent probe**

Exploring binding with CL is crucial for screening new, CL-targeted modulators of mitochondrial functions and antibiotics, as well as for evaluating drugs` potential to cause mitochondrial toxicity by interacting with CL.

In the early 1980s a fluorescent dye, 10-*N*-nonyl acridine orange (NAO), was introduced for selective CL detection and mitochondria staining (Mileykovskaya et al., 2001). However, NAO has significant drawbacks and, therefore, a limited use as a probe for both quantitative analysis and competition assays – fluorescence intensity of NAO is relatively low and unstable due to low solubility in aqueous medium, low photoluminescence quantum yield ( $\Phi$ ) and

small intensity differences between CL-bound and unbound states. Another commercially available CL-specific fluorescent probe, TTape-Me, forms a fluorescent complex with CL, but its fluorescence intensity is also very low (Chen et al., 2015); hence, a large amount of both sample and probe is necessary for obtaining qualitative results. Another major disadvantage of TTape-Me is its binding mode – it binds with CL only electrostatically and sodium ions compete with the probe, making it unusable for competitive binding studies.

Therefore, there is a great demand for a more stable and sensitive CL-specific probe for CL concentration measurements as well as for a robust method for rapid biologically active compound screening for CL targeting and quantitative binding affinity characterisation. For this reason, improvements should be made in a fluorescent probe's solubility, stability, photoluminescence quantum yield and fluorescence intensity.

### **1.2.1 Synthesis of the new cardiolipin-specific fluorescent probes**

To overcome the issues mentioned above, the research was focused on improving the physicochemical properties of NAO. Firstly, solubility and stability issues were addressed. It was known that N<sup>+</sup> cation is crucial for the probe's interaction with phosphate groups of CL, at the same time, alkyl chain should retain lipophilicity to form hydrophobic bonds with CL's fatty acid chains (Rodriguez et al., 2008). Obviously, the hydrophobic alkyl chain of NAO negatively impacts its solubility and for this reason was chosen for modification.

Alkylation of acridine orange proceeds slowly (24–72 h) with low conversion and is accompanied by the formation of many side products, that can be explained by 3,6-dimethylamino acridinium salts demethylation under prolonged heating. To produce more active alkylating agents for the reduction of the reaction time and heat exposure of the starting materials, *in situ* formed dialkyl carbonates, sulphates and trialkyl phosphates were tested in toluene,

xylene and dichlorobenzene under reflux. Surprisingly, it was found that AO quaternisation with 1-bromononane or 1-iodononane in dichlorobenzene at 170 °C in the presence of 2 equiv. Na<sub>2</sub>CO<sub>3</sub> resulted in 91 and 98 % conversion, respectively, without a significant amount of demethylated by-products (Figure 1.6). This method allowed to obtain quaternised acridinium salts in good yields and with high purity (≥ 96.5 %, HPLC).

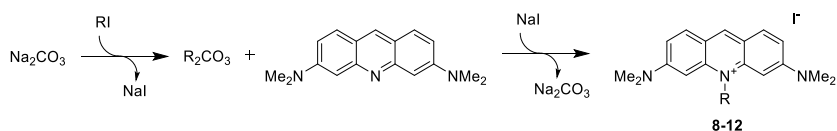


Figure 1.6 Synthesis of compounds 8–12\*

\*Reaction conditions: alkyl iodide, dichlorobenzene, 170 °C, Na<sub>2</sub>CO<sub>3</sub> (2 equiv.).

**8**, R = methyl, 98 %; **9**, NAO, R = nonyl, 77 %; **10**, R = dodecyl, 76 %;

**11**, R = 3-(trimethylsilyl)propyl, 97 %; **12**, R = 3-silatranylpropyl, 14 %.

To increase the solubility of a probe in aqueous medium without losing lipophilicity, (3-iodopropyl) trimethylsilane was used. The obtained 3-(trimethylsilyl)propyl substituted acridinium iodide **12** had 5-fold higher solubility in 20 mM HEPES (pH = 7.4) compared to NAO and better stability after 24 h. Furthermore, the introduction of the 3-(trimethylsilyl)propyl substituent led to a slight increase in  $\Phi$  compared to NAO (18.7 % and 15.5 %, respectively); however, this small increase in  $\Phi$  resulted in ~30 % increase in fluorescence intensity (FI).

It has been shown in similar heterocyclic systems that an azetidiny group significantly improves  $\Phi$ , presumably by hindering twisting of the C<sub>aryl</sub>-N bond and disfavours the formation of a twisted internal charge transfer state (Grimm et al., 2015). To confirm this, replacement of dimethylamino groups with cyclic amino substituents in positions 3 and 6 of the acridinium salt structure was performed. First, compounds **14–17** were synthesised using palladium-catalysed

cross-coupling of **13** with cyclic amines and then alkylated using the previously developed method with the corresponding alkyl iodide in the presence of sodium carbonate to obtain acridinium iodides **18–25** (Figure 1.7).

As expected, azetidinyl AO analogues **18–20** exhibited a 4-fold higher  $\Phi$  ( $\approx 60\%$ ) than NAO (Table 1.2). Pyrrolidyl-substituted acridinium salt **23** displayed moderate  $\Phi$  (40%), but piperidyl and morpholyl analogues **24** and **25** had very low  $\Phi$ , 2.7% and 6.8%, respectively.

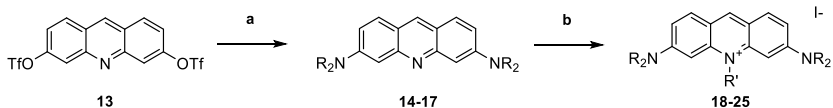


Figure 1.7 Synthesis of acridinium salts **18–25**\*


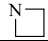

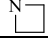
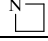
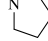
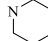
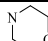
\*Reaction conditions: a) cyclic amine (3 equiv.), Pd(OAc)<sub>2</sub> (25 mol-%), BINAP (30 mol-%), Cs<sub>2</sub>CO<sub>3</sub> (4 equiv.), xylene, reflux, 16h; b) R'-I, Na<sub>2</sub>CO<sub>3</sub>, dichlorobenzene or toluene, reflux, 10-40 min. **14**, NR<sub>2</sub> = azetidinyl, 69%; **15**, NR<sub>2</sub> = pyrrolidyl, 54%; **16**, NR<sub>2</sub> = piperidyl, 65%; **17**, NR<sub>2</sub> = morpholyl, 67%; **18**, NR<sub>2</sub> = azetidinyl, R' = CH<sub>3</sub>, 75%; **19**, NR<sub>2</sub> = azetidinyl, R' = CD<sub>3</sub>, 89%; **20**, NR<sub>2</sub> = azetidinyl, R' = Me<sub>3</sub>Si(CH<sub>2</sub>)<sub>3</sub>, 61%; **21**, NR<sub>2</sub> = azetidinyl, R' = C<sub>9</sub>H<sub>19</sub>, 76%; **22**, NR<sub>2</sub> = azetidinyl, R' = C<sub>12</sub>H<sub>25</sub>, 54%; **23**, NR<sub>2</sub> = pyrrolidyl, R' = Me<sub>3</sub>Si(CH<sub>2</sub>)<sub>3</sub>, 98%; **24**, NR<sub>2</sub> = piperidyl, R' = Me<sub>3</sub>Si(CH<sub>2</sub>)<sub>3</sub>, 59%; **25**, NR<sub>2</sub> = morpholyl, R' = Me<sub>3</sub>Si(CH<sub>2</sub>)<sub>3</sub>, 63%.

Azetidinyl-substituted analogues with methyl and 3-(trimethylsilyl)propyl group displayed the highest  $\Phi$ , and the elongation of the alkyl chain at position 10 led to the decrease of  $\Phi$ . Therefore, azetidinyl-substituted acridinium iodides **18** and **20** were selected for further studies.

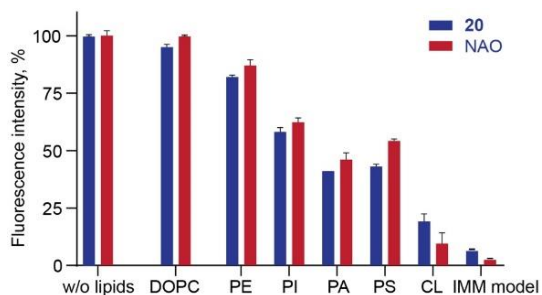
As was supposed, in the absence of a hydrophobic alkyl chain, N-methyl-substituted diazetidinyl acridinium **18** did not form a stable complex with CL, which was confirmed by a 13% increase in FI in 10 min after the addition of the compound to CL.

Table 1.2

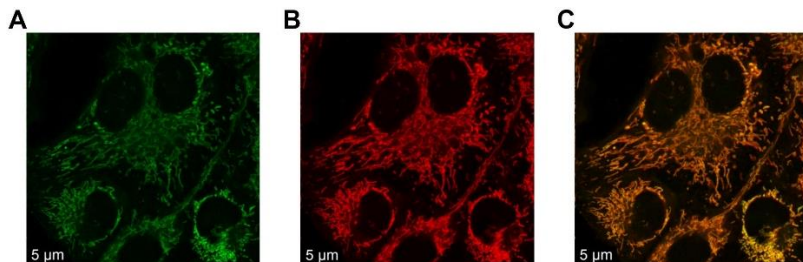
## Photoluminescence properties of NAO analogues

Compound	R	R'	$\Phi$ , %	$\lambda_{\text{abs}}/\lambda_{\text{em}}$ , nm
<b>9 (NAO)</b>	Me <sub>2</sub> N	C <sub>9</sub> H <sub>19</sub>	15.5	497/529
<b>12</b>	Me <sub>2</sub> N	Me <sub>3</sub> Si(CH <sub>2</sub> ) <sub>3</sub>	18.7	491/529
<b>18</b>		CH <sub>3</sub>	59.9	498/529
<b>19</b>		CD <sub>3</sub>	61.5	498/529
<b>20</b>		Me <sub>3</sub> Si(CH <sub>2</sub> ) <sub>3</sub>	60.7	497/529
<b>21</b>		C <sub>9</sub> H <sub>19</sub>	47.9	498/529
<b>22</b>		C <sub>12</sub> H <sub>25</sub>	16.1	496/529
<b>23</b>		Me <sub>3</sub> Si(CH <sub>2</sub> ) <sub>3</sub>	40.0	511/529
<b>24</b>		Me <sub>3</sub> Si(CH <sub>2</sub> ) <sub>3</sub>	2.7	484/547
<b>25</b>		Me <sub>3</sub> Si(CH <sub>2</sub> ) <sub>3</sub>	6.8	488/547

In turn, the FI of compound **20** and its complex with CL was stable in buffer for at least 30 min, in contrast to NAO. This fact could be explained by approx. 5-fold higher solubility of compound **20** (0.188 mg/ml versus 0.041 mg/ml for NAO). It is important to note that compound **20** retained the same specificity toward CL as NAO (Figure 1.8).

Figure 1.8 Interaction of compound **20** and NAO with phospholipids

Moreover, compound **20** was successfully implemented in live cell imaging of mitochondria (Figure 1.9). For comparison, MitoTracker deep red, a commercially available dye for mitochondria staining, was applied to confirm mitochondrial localisation of compound **20**.



**Figure 1.9 A) Subcellular localisation of **20** (100 nM) in human melanoma cells (A2058); B) Mitochondria in A2058 cells stained with MitoTracker deep red (200 nM); C) Representative colocalisation of **20** and MitoTracker deep red**

The fluorescent signal of compound **20** precisely overlapped with MitoTracker deep red and did not significantly spread to other organelles.

Consequently, compound **20** was chosen as a fluorescent probe for the quantitative analysis of CL and for the development of an assay to measure the binding affinity of biologically active substances for CL.

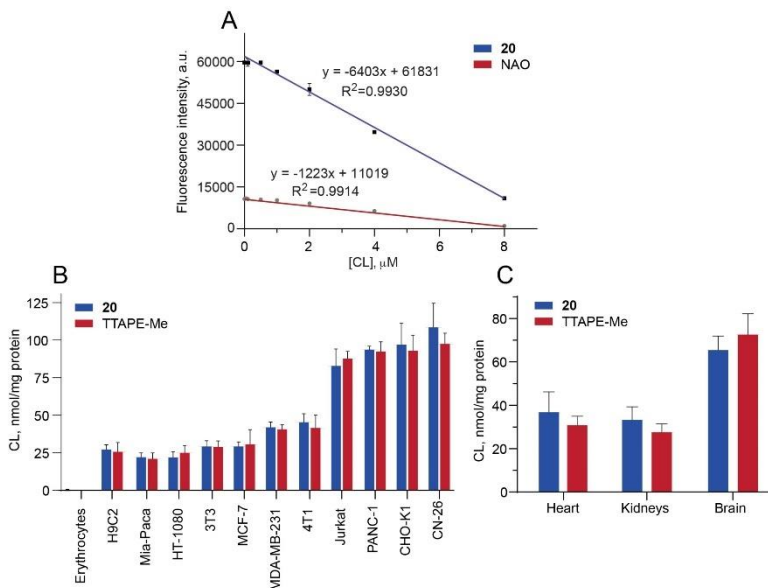
### **1.2.2 Cardiolipin quantitative analysis**

First, a quantitative analysis of CL was performed in a CL/DOPC liposomal model: compound **20** was titrated with CL in the 0.05–8  $\mu\text{M}$  range, and a linear regression curve ( $R^2 = 0.9930$ ) was obtained (Figure 1.10 A). Next, since CL is almost exclusively located in mitochondria, the amount of CL was measured in mitochondrial fractions isolated from different cell lines using calibration curves obtained with liposomal CL solutions. Human erythrocyte lysate was taken as a negative control because human erythrocytes do not have



no mitochondria and, therefore, do not have CL. In parallel, CL concentration was measured with TTAPE-Me and compared with the results obtained with compound **20** using Student's *t*-test (Figure 1.10 B). In all cell lines studied, no statistically significant difference ( $p > 0.37$ , Student's *t*-test) in the determined CL concentration was found using compound **20** or TTAPE-Me. Moreover, in erythrocytes, no CL was detected, thus confirming the selectivity of compound **20** for CL.

Cardiomyoblasts (H9C2) are considered rich in mitochondria and contain a relatively large amount of CL ( $26.6 \pm 3.7$  nmol/mg prot). Strikingly, cancer cell lines and cell lines with high proliferation rates contain comparable or even higher amounts of CL.



**Figure 1.10 A) **20** and NAO (16  $\mu\text{M}$ ) titration with CL/DOPC liposomes in 20 mM HEPES, pH = 7.4; B) CL amount in mitochondrial fractions from cell lysates; C) CL amount in mitochondrial fractions from C57Bl/6J mice tissue homogenates\***

\*n = 3–5. In all cases  $p > 0.05$  (Student's *t*-test).

The highest concentration of CL among the studied cell lines,  $108.5 \pm 16.0$  nmol/mg prot., was found in the mitochondria of mouse colon carcinoma cells (CT-26), which is consistent with published data on elevated CL levels in colon cancer (Zichri et al., 2021).

The next step was to confirm whether it is possible to measure CL concentration in mitochondrial fractions isolated from animal tissue. Mitochondrial fractions were isolated from healthy C57Bl/6J mouse heart, kidney and brain tissue homogenates, and CL content was analysed by the same method as previously described (Figure 1.10 C). No statistically significant differences were found between CL concentrations obtained by compound **20** or TTape-Me ( $p > 0.44$ , Student's *t*-test). The mouse heart and kidney mitochondria contained similar amounts of CL,  $37.49 \pm 8.69$  and  $33.95 \pm 5.32$  nmol/mg prot., respectively. Previously reported CL concentrations of 15–20 nmol/mg prot. for mouse heart mitochondria (Grevengoed et al., 2015; Pennington et al., 2019) could be underestimated due to the possible loss of CL during lipid extraction and separation procedures. Remarkably, CL concentration in mouse brain mitochondria ( $66.11 \pm 5.78$  nmol/mg prot.) was almost twice that of the heart and kidneys. The obtained value was slightly higher than the previously reported value ( $52.7 \pm 4.5$  nmol/mg prot.) (Kiebish et al., 2009), which could also be explained by the lipid extraction step before CL quantification or CL level fluctuations between different mouse strains.

In summary, the developed fluorescent dye **20** is suitable for the fast and straightforward measurement of CL concentrations in mitochondrial fractions isolated from cultured cells and animal tissues. The greatest advantages are the simplicity of the procedure (lipid extraction and separation are not necessary), only 15 min incubation and a single-point emission measurement, that produces a clear and stable response. Although the developed assay allows quantification

of the total amount of CL, its limitation is the inability to distinguish between CL species with different alkyl chain compositions.

### 1.2.3 Fluorescence-based competitive binding assay

Cytochrome c (cyt c), an endogenous CL ligand, and CL/DOPC liposomes (25:75 mol %) were selected for the development and optimisation of the experimental procedure. The most pronounced response was when compound **20** and CL were used in a saturating ratio of 2:1 at 5 and 2.5  $\mu\text{M}$  concentrations, respectively. Cyt c showed high affinity for CL, and at pH 7.4 had  $\text{EC}_{50}$  value of  $0.32 \pm 0.06 \mu\text{M}$  (Figure 1.11 A).

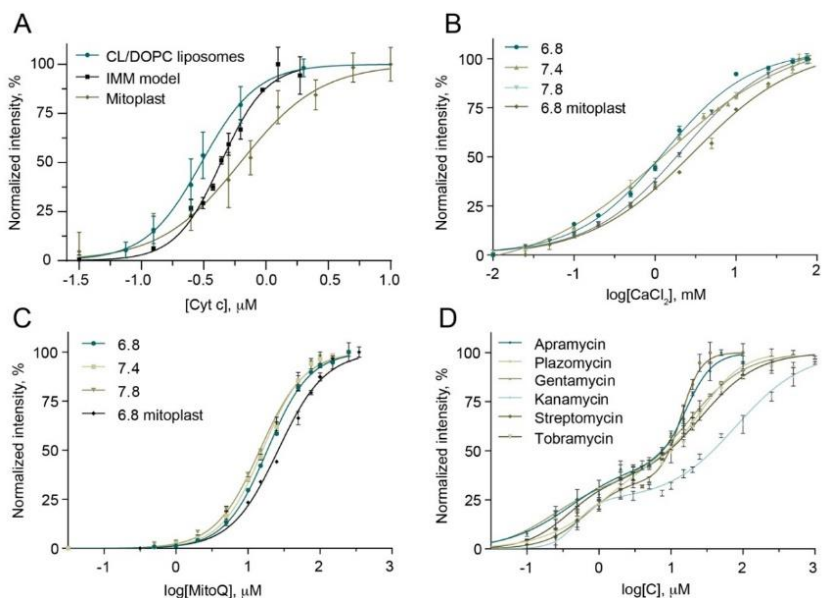


Figure 1.11 A) Cyt c binding with CL in CL/DOPC liposomes, IMM model and mitoplasts; B) Representative curves of  $\text{CaCl}_2$  and mitoQ binding with CL in CL/DOPC liposomes and isolated mitoplasts; C) Aminoglycosides' binding with CL in CL/DOPC liposomes

A similar  $EC_{50}$  value ( $0.44 \pm 0.02 \mu\text{M}$ ) was obtained in experiments in a more complex model of the IMM (PI, CL, PE and DOPC, 10:25:30:35 mol %). Therefore, simple CL/DOPC liposomes were selected as a more simple and cheaper artificial membrane model for the screening purpose. Mitoplasts isolated from a rat heart, representing a natural lipid membrane, were also successfully applied. In this case, cyt c had an approx. twofold higher  $EC_{50}$  value ( $0.78 \pm 0.15 \mu\text{M}$ ), probably because of the interaction with other IMM components such as intermembrane proteins or other lipids. Next, the ability of cyt c to bind to CL was evaluated at different pH values representing the mitochondrial intermembrane space (6.8), cytosol (7.4), and mitochondrial matrix (7.8) (Santo-Domingo and Demareux, 2012). The results also confirmed that the affinity of cyt c for CL is independent of pH.

Considering the strong and pH-independent binding of cyt c as well as its commercial availability, cyt c can be proposed as a reference compound. To validate the method, different ligands were studied (Figure 1.11 B–D and Table 1.3).

In total, the assay was validated by testing 25 substances of different nature – inorganic salts, peptide, glycopeptide, polycationic sugars, lipophilic phosphonium and ammonium salts, drugs containing guanine and guanidine moieties, and other substances. The developed procedure does not require special equipment other than a fluorimeter and is time-efficient, which makes it suitable for screening a large number of compounds. In general, positively charged substances bind to CL, but their affinity varies markedly; the  $EC_{50}$  values lie in the sub-micromolar to millimolar range. The interaction of the fluorescent probe with the studied compounds, e.g., heavy metal ions, is a limitation of the assay; therefore, a blank titration without CL must always be performed to avoid misinterpretation of the results.

Table 1.3

## Compounds relative affinity toward CL

EC <sub>50</sub> , μM				
Model	CL/DOPC	CL/DOPC	CL/DOPC	Mitoplasts
pH	6.8	7.4	7.8	6.8
<b>Inorganic salts</b>				
MgCl <sub>2</sub>	1141 ± 122	1102 ± 66	1300 ± 94	1576 ± 190
Zn gluconate	683 ± 111	736 ± 37	344 ± 32	792 ± 125
CaCl <sub>2</sub>	1285 ± 129	1334 ± 101	1701 ± 154	2703 ± 246
NH <sub>4</sub> Cl	14849 ± 2002; 88827 ± 3392	14270 ± 165; 45130 ± 153	9170 ± 149; 82020 ± 130	4930 ± 107; 68290 ± 810
NaCl	> 100000	> 100000	> 100000	> 100000
HgCl <sub>2</sub>	q	q	q	q
<b>Compounds that affect mitochondrial function</b>				
Cytochrome c	0.26 ± 0.02	0.32 ± 0.06	0.33 ± 0.06	0.78 ± 0.15
Nonyl TPP	36.65 ± 2.93	19.76 ± 0.75	28.82 ± 1.02	43.31 ± 3.87
MitoQ	19.55 ± 1.67	15.92 ± 0.87	17.06 ± 0.17	30.67 ± 5.14
Metformin	> 500	> 500	> 500	n.t.
Thimerosal	> 500	> 500	> 500	n.t.
Acyclovir	> 500	> 500	> 500	n.t.
Abacavir	> 500	> 500	> 500	n.t.
Antimycin A	q	q	q	n.t.
CCCP	q	q	q	n.t.
<b>Antibiotics</b>				
Vancomycin	796 ± 47	434 ± 62	346 ± 21	1732 ± 29
Rifampicin	q	q	q	n.t.
Ampicillin Na	> 500	> 500	> 500	n.t.
Dodecyl trimethyl- ammonium chloride	74.41 ± 8.47	30.71 ± 2.75	23.16 ± 2.74	69.20 ± 3.67
Apramycin	0.85 ± 0.04; 102.5 ± 1.5	0.63 ± 0.21; 14.54 ± 0.59	0.58 ± 0.04; 27.87 ± 2.70	2.79 ± 0.31; 593 ± 76
Gentamycin	1.04 ± 0.09; 384 ± 18	0.22 ± 0.03; 19.19 ± 1.44	0.38 ± 0.05; 24.15 ± 3.90	1.83 ± 0.69; 298 ± 55
Streptomycin	1.22 ± 0.20; 87.5 ± 6.2	0.60 ± 0.15; 14.15 ± 2.17	0.89 ± 0.12; 16.28 ± 2.83	2.33 ± 0.05; 155 ± 69
Tobramycin	n.t.	0.40 ± 0.16; 26.16 ± 2.79	n.t.	n.t.
Kanamycin	n.t.	0.44 ± 0.10; 80.1 ± 13.5	n.t.	n.t.
Plazomicin	n.t.	1.13 ± 0.46; 29.4 ± 4.2	n.t.	n.t.

\*n.t. – not tested, q- fluorescence of compound **20** is quenched by a studied compound.

## 1.2.4 Isoselenazolium salts affinity for cardiolipin

After the development of the new method, it was finally possible to measure the affinity of isoselenazolium salts for CL. Despite the previous data obtained by ITC showing a clear exothermic interaction between compound **6** and CL containing liposomes, both compounds **6** and **3** tested in the CL/DOPC model had  $EC_{50} > 500 \mu\text{M}$ , which means that their affinity for CL is low, and it is unlikely that their impact on mitochondrial respiration and overall cytotoxic effect is exerted through interaction with CL. Therefore, it was decided to modify isoselenazolium salt's structure, and focus studies on pyruvate-dependent mitochondrial respiration,  $\text{NAD}^+$  metabolism and PARP1 inhibitory activity.

## 1.3 The second generation of isoselenazolium salts and their mechanism of action

### 1.3.1 Synthesis of new isoselenazolium derivatives

The original plan was to introduce the nicotinamide moiety in the isoselenazolopyridinium core to resemble to some extent a part of the  $\text{NAD}^+$  structure, which is a substrate for PARP1, and study the impact of the amide, carboxyl and methyl ester group on cytotoxicity (Figure 1.12).

The synthetic route started from  $\alpha$ -bromopyridines **26a–c**, that were treated with 1-ethynyl-1-cyclohexanol in the presence of palladium catalyst to produce ethynyl-substituted derivatives **27a–c** in high yields. The corresponding carboxylic acids were obtained by hydrolysis of the ester group of compounds **28a–c** with NaOH, and amides **29a–c** were synthesised in reaction of compounds **27a–c** with saturated methanolic solution of  $\text{NH}_3$ . Methyl- $d_3$  2-((1-hydroxycyclohexyl)ethynyl) isonicotinate (**27d**) was prepared by treating a suspension of the compound **28c** and  $\text{CD}_3\text{OD}$  with HOBt hydrate and EDC·HCl in DMF.

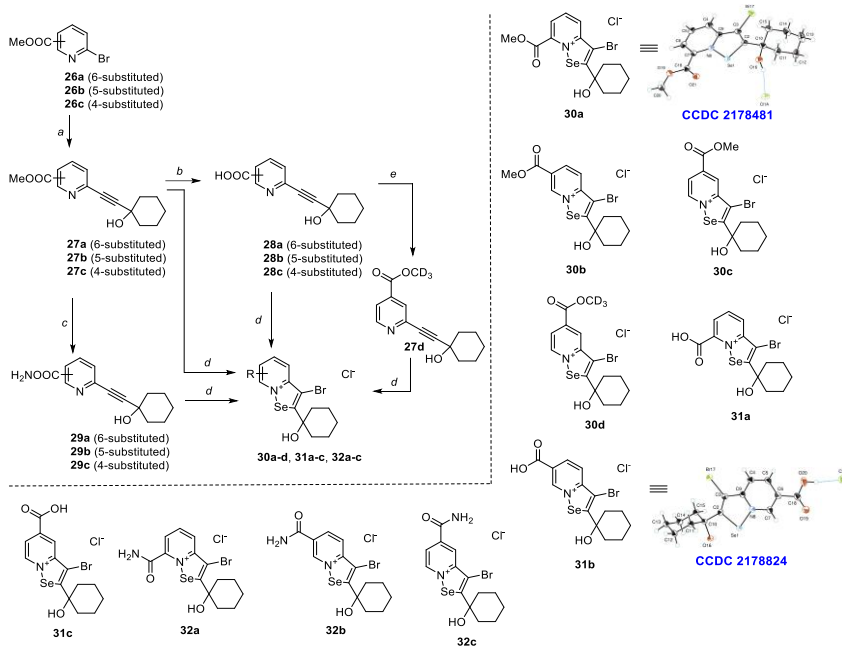


Figure 1.12 **Synthesis of isoselenazopyridinium chlorides 30a–e, 31a–c and 32a–c\***

- \*Reaction conditions: a) terminal acetylene (1.4 equiv.), CuI (0.01–0.05 equiv.),  $(\text{Ph}_3\text{P})_2\text{PdCl}_2$  (0.01–0.05 equiv.), DMF/ $i\text{Pr}_2\text{NH}$  or  $\text{Et}_3\text{N}$ , 50 or 80 °C, 2–5 h; b) 1. NaOH (5 equiv.), 2. HCl, MeOH/ $\text{H}_2\text{O}$ , rt, overnight; c)  $\text{NH}_3$ , MeOH, rt, overnight; d)  $\text{SeBr}_4$ , dioxane/water, rt; e)  $\text{CD}_3\text{OD}$ , EDC·HCl, HOBT· $\text{H}_2\text{O}$ , DMF, rt, 2 h.

After obtaining all derivatives of ethynyl pyridines, the corresponding isoselenazolium salts were synthesised based on a previously established procedure (Arsenyan et al., 2015). Ethynyl pyridines **27a–d**, **28a–c** and **29a–c** were treated with *in situ* prepared  $\text{SeBr}_4$  by dissolving selenium(IV) oxide in the concentrated hydrobromic acid in dioxane/water. After consumption of a substrate, the crude material was dissolved in the ethanol/water mixture and eluted through ion-exchange resins pretreated with hydrochloric acid to produce isoselenazopyridinium chlorides **30a–d**, **31a–c** and **32a–c**. However, the treatment of 2-((1-hydroxycyclohexyl)ethynyl)nicotinic acid as well as its amide

and methyl ester derivatives with  $\text{SeBr}_4$  was unsuccessful and resulted in only traces of the desired products.

Based on preliminary structure-activity relationship (SAR) data, cyclohexyl substituent at position 2 was replaced by cyclobutyl, cyclopentyl, adamantyl, tridecyl and difluorocyclohexyl groups. Isoselenazolypridinium chlorides **30f–k**, **32d–f** were synthesised similarly to the previous set of compounds (Figure 1.13). Compounds **30j** and **30k** were synthesised using methyl- and fluoro- substituted pyridine bromides as a starting material. The molecular structures of compounds **30a** (CCDC 2178481), **30e** (CCDC 2179108), **31b** (CCDC 2178824), and **32e** (CCDC 2178826) were confirmed by X-ray diffraction.

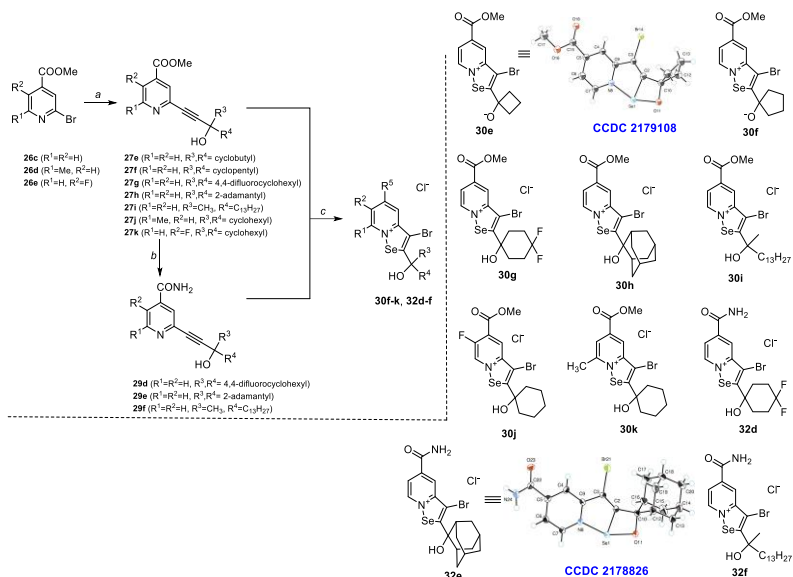


Figure 1.13 Synthesis of isoselenazolypridinium chlorides **30f–k** and **32d–f**\*

\*Reaction conditions: a) terminal acetylene (1.4 equiv.), CuI (0.01–0.05 equiv.),  $(\text{Ph}_3\text{P})_2\text{PdCl}_2$  (0.01–0.05 equiv.), DMF/ $i\text{Pr}_2\text{NH}$  or  $\text{Et}_3\text{N}$ , 50 or 80 °C, 2–5 h; b)  $\text{NH}_3$ , MeOH, rt, overnight; c)  $\text{SeBr}_4$ , dioxane/water, rt.



### 1.3.2 Cytotoxicity of the new isoselenazolium derivatives

The cytotoxicity of new isoselenazolium salts was studied in human and mouse breast cancer (MCF-7, MDA-MB-231, 4T1), T cell leukaemia (Jurkat), human hepatocellular carcinoma (HCC1937) and human lung adenocarcinoma (A549) cells, and the data are summarised in Table 1.4. As the new compounds were likely to modulate mitochondrial function, rat cardiomyoblasts (H9C2) were selected as a control normal cell line because they contain a large number of mitochondria (Kuznetsov et al., 2015) and are widely used to assess mitochondrial toxicity *in vitro* (Kim and Choi, 2021).

The carboxyl group in the isoselenazolopyridinium ring (compounds **31c** and **31b**) reduced cytotoxicity and selectivity toward cancer cells, probably, because of the poor solubility and low cell permeability. Compounds **30a** and **31a** were excluded from the study due to low solubility in aqueous medium. In turn, derivatives with the methoxy carbonyl or amide group in positions 5 or 6 exhibited high cytotoxicity toward a wide range of malignant cell lines. In particular, compound **30c** with the methoxy carbonyl group at position 5 stood out with a favourable cytotoxicity profile. In turn, the introduction of fluorine atom in position 6 or methyl group in position 7 reduced selectivity toward cancer cells. Then, substituents at position 2 were modified, and it was concluded that bulky (adamantyl) or lipophilic (2-hydroxypentadecan-2-yl) substituents reduce cytotoxicity and/or selectivity toward cancer cells. It was found that the optimal substituent is 1-hydroxycyclohexyl group, and cytotoxicity for most of the cell lines decreased with a smaller number of carbon atoms in the hydroxycycloalkane ring.

While some analogues, such as **30g** and **30f**, were worth mentioning, compound **30c** was the most selective and exhibited the highest cytotoxic activity in a wider spectrum of cancer cell lines. Hence, compound **30c** was selected to study the mechanism of action.

Table 1.4

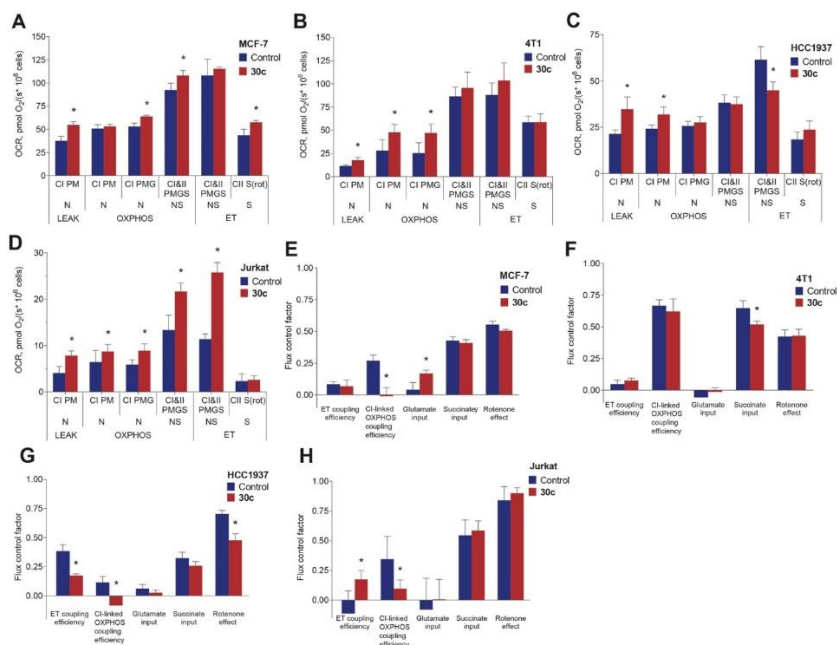
## Cytotoxic activity of compounds 30b–32f against cancer cell lines and cardiomyoblasts

Compound	Cytotoxicity, IC <sub>50</sub> , $\mu$ M							
	H9C2	Jurkat	MCF7	HCC1937	A549	MDA-MB-231	4T1	
Doxorubicin	3.90 $\pm$ 0.60	0.32 $\pm$ 0.08	0.47 $\pm$ 0.14	1.08 $\pm$ 0.10	0.23 $\pm$ 0.07	0.41 $\pm$ 0.08	0.065 $\pm$ 0.008	
<b>30b</b>	0.89 $\pm$ 0.27	0.25 $\pm$ 0.06	0.87 $\pm$ 0.29	0.31 $\pm$ 0.11	1.31 $\pm$ 0.20	0.43 $\pm$ 0.14	0.70 $\pm$ 0.18	
<b>30c</b>	2.46 $\pm$ 0.60	0.44 $\pm$ 0.25	1.16 $\pm$ 0.09	0.33 $\pm$ 0.03	1.30 $\pm$ 0.23	0.51 $\pm$ 0.15	0.32 $\pm$ 0.03	
<b>30d</b>	0.64 $\pm$ 0.28	0.49 $\pm$ 0.06	0.38 $\pm$ 0.09	0.54 $\pm$ 0.02	1.20 $\pm$ 0.46	0.40 $\pm$ 0.11	1.11 $\pm$ 0.04	
<b>30e</b>	2.97 $\pm$ 0.22	3.24 $\pm$ 0.49	2.80 $\pm$ 0.75	3.03 $\pm$ 0.40	9.12 $\pm$ 1.42	6.51 $\pm$ 0.67	>10	
<b>30f</b>	0.77 $\pm$ 0.14	0.48 $\pm$ 0.22	0.36 $\pm$ 0.13	0.41 $\pm$ 0.13	8.70 $\pm$ 1.43	1.66 $\pm$ 0.35	2.04 $\pm$ 0.60	
<b>30g</b>	1.06 $\pm$ 0.03	0.48 $\pm$ 0.27	0.28 $\pm$ 0.13	0.24 $\pm$ 0.10	1.16 $\pm$ 0.25	0.48 $\pm$ 0.13	1.48 $\pm$ 0.44	
<b>30h</b>	4.76 $\pm$ 0.18	6.18 $\pm$ 0.16	6.87 $\pm$ 0.75	2.89 $\pm$ 0.37	n.t.	n.t.	n.t.	
<b>30i</b>	3.63 $\pm$ 0.38	3.38 $\pm$ 0.30	3.79 $\pm$ 0.57	2.45 $\pm$ 0.43	n.t.	n.t.	n.t.	
<b>30j</b>	1.68 $\pm$ 0.36	1.16 $\pm$ 0.19	1.08 $\pm$ 0.02	1.19 $\pm$ 0.27	2.93 $\pm$ 0.47	1.38 $\pm$ 0.40	2.34 $\pm$ 0.51	
<b>30k</b>	0.90 $\pm$ 0.24	0.45 $\pm$ 0.11	0.30 $\pm$ 0.18	0.34 $\pm$ 0.05	1.12 $\pm$ 0.26	0.37 $\pm$ 0.14	0.96 $\pm$ 0.14	
<b>31b</b>	3.55 $\pm$ 0.18	3.26 $\pm$ 0.54	> 10	3.85 $\pm$ 0.61	n.t.	n.t.	n.t.	
<b>31c</b>	7.82 $\pm$ 0.19	6.61 $\pm$ 2.15	> 10	5.82 $\pm$ 0.72	7.03 $\pm$ 0.10	6.12 $\pm$ 0.47	6.81 $\pm$ 0.33	
<b>32a</b>	2.63 $\pm$ 0.44	1.88 $\pm$ 0.42	3.85 $\pm$ 0.41	1.33 $\pm$ 0.30	n.t.	n.t.	n.t.	
<b>32b</b>	1.27 $\pm$ 0.13	0.60 $\pm$ 0.25	2.30 $\pm$ 0.87	1.50 $\pm$ 0.34	n.t.	n.t.	n.t.	
<b>32c</b>	1.41 $\pm$ 0.17	1.00 $\pm$ 0.15	2.22 $\pm$ 0.57	0.60 $\pm$ 0.25	2.81 $\pm$ 0.58	1.15 $\pm$ 0.20	1.41 $\pm$ 0.28	
<b>32d</b>	1.41 $\pm$ 0.26	1.43 $\pm$ 0.36	1.00 $\pm$ 0.08	0.60 $\pm$ 0.25	3.17 $\pm$ 0.23	1.36 $\pm$ 0.18	1.25 $\pm$ 0.08	
<b>32e</b>	0.91 $\pm$ 0.25	0.91 $\pm$ 0.29	0.61 $\pm$ 0.04	0.74 $\pm$ 0.26	2.21 $\pm$ 0.36	0.65 $\pm$ 0.21	0.56 $\pm$ 0.02	
<b>32f</b>	1.91 $\pm$ 0.55	2.00 $\pm$ 0.25	1.01 $\pm$ 0.08	0.91 $\pm$ 0.10	3.72 $\pm$ 0.40	2.42 $\pm$ 0.18	4.32 $\pm$ 0.73	

\*Values are shown as the means  $\pm$  SD from 3–5 independent experiments. n.t. = not tested.

### 1.3.3 Influence on mitochondrial respiration, ROS production and coupling state of the electron transfer system

The impact of compound **30c** on mitochondrial respiration was studied in HCC1937, MCF-7, 4T1 and Jurkat cells by high-resolution respirometry (Figure 1.14).



**Figure 1.14 The effect of compound 30c at 1  $\mu$ M concentration on mitochondrial respiration. Respiratory parameters in permeabilised (A) MCF-7, (B) 4T1, (C) HCC1937, (D) Jurkat cells. Flux control factors in permeabilised (E) MCF-7, (F) 4T1, (G) HCC1937, (H) Jurkat cells\***

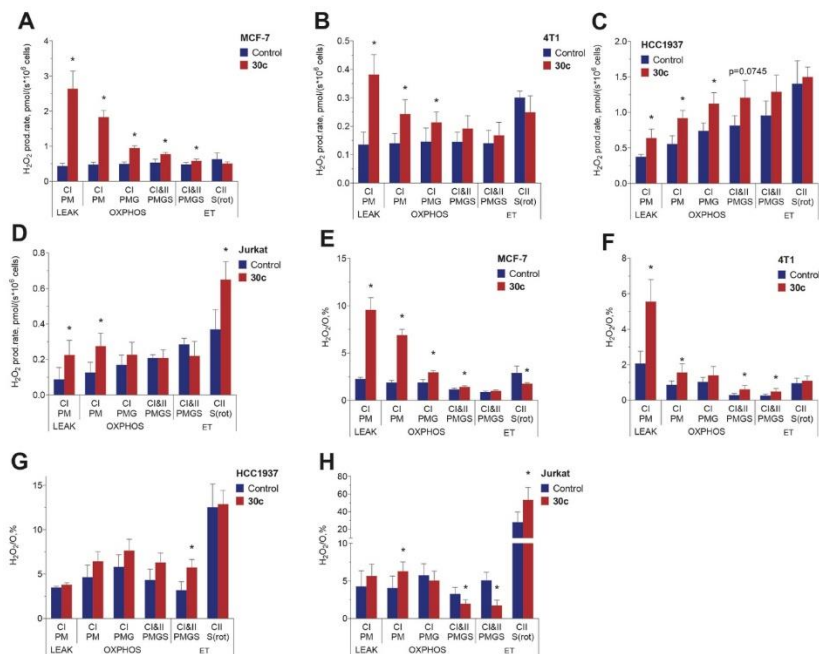
\*OCR – oxygen consumption rate; CI – complex I; CII – complex II; LEAK – substrate dependent respiration rate; OXPHOS – oxidative phosphorylation dependent state; ET – electron transfer, uncoupled state; P – pyruvate; M – malate; G – glutamate; S – succinate; N – NADH-generating substrates; NS – NADH and succinate generating substrates; rot – rotenone. Statistically significant difference (\*) was considered when  $p < 0.05$  (Students *t*-test) compared to the control group (vehicle-DMSO).

These cell lines showed significant differences in mitochondrial metabolic activity, and their maximal oxygen consumption rate (OCR) was in the following descending order: MCF-7 > 4T1 > HCC1937 > Jurkat (Figure 1.14 A–D).

Surprisingly, compound **30c** significantly increased OCR in all cell lines in the presence of pyruvate and malate in LEAK, OXPHOS or both states. However, **30c** abruptly interrupted OXPHOS coupling in the presence of CI substrates (pyruvate and malate) in MCF-7 (Figure 1.14 E), HCC1937 (Figure 1.14 G) and Jurkat (Figure 1.14 H), but not in 4T1 cells (Figure 1.14 F). Compound **30c** does not appear to have a direct impact on CI because the effect of rotenone (CI inhibitor) was almost identical in the treatment and control groups, except for HCC1937, where the effect of rotenone was reduced. In addition, there were no substantial changes in mitochondrial function in the CII-linked OXPHOS state. Elevated OCR can be explained by the increase in ROS production. Immediately after addition of compound **30c** there was a massive increase in the rate of H<sub>2</sub>O<sub>2</sub> production in all cell lines. (Figure 1.15 A–D).

The most pronounced H<sub>2</sub>O<sub>2</sub> production spikes were in the presence of CI substrates. Higher H<sub>2</sub>O<sub>2</sub>/O ratios (Figure 1.15 E–H) indicate that more oxygen was shifting toward ROS production rather than participating in ETS.

The increase in mitochondrial ROS production may arise from CI or complex III (CIII) produced superoxide anion. However, the production of O<sub>2</sub><sup>•-</sup> by CIII is generally low and it is unlikely to be associated with such significant effects (Forman and Azzi, 1997). In turn, CI can produce a large amount of O<sub>2</sub><sup>•-</sup> and H<sub>2</sub>O<sub>2</sub> during both forward (NADH-oxidizing) and reverse (NAD<sup>+</sup>-reducing) electron transport. The latter can be ruled out, because the upsurge of H<sub>2</sub>O<sub>2</sub> production is not levelled out by rotenone, confirming that electrons do not enter into CI through the coenzyme Q-binding site(s) in the opposite direction (Murphy, 2009).



**Figure 1.15 Effect of 1  $\mu$ M 30c on H<sub>2</sub>O<sub>2</sub> production rate in permeabilised (A) MCF-7, (B) 4T1, (C) HCC1937 and (D) Jurkat cells. H<sub>2</sub>O<sub>2</sub>/O<sub>2</sub> ratio in permeabilised (E) MCF-7, (F) 4T1, (G) HCC1937 and (H) Jurkat cells\***

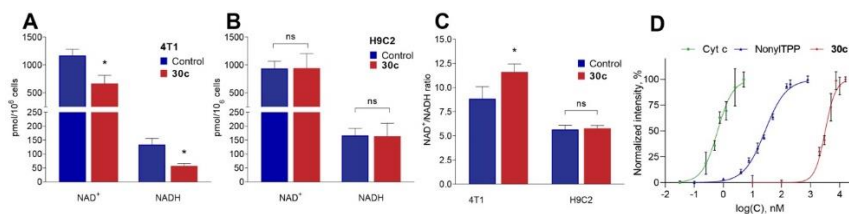
\*CI – complex I; CII – complex II; LEAK – substrate dependent respiration rate;

OXPHOS – oxidative phosphorylation dependent state; ET – electron transfer, uncoupled state; P – pyruvate; M – malate; G – glutamate; S – succinate; rot – rotenone. Values are shown as mean  $\pm$  SD. Statistically significant difference (\*) was considered when  $p < 0.05$  (Students *t*-test) compared to the control group (vehicle-DMSO).

Another way to induce mitochondrial ROS production is by decreasing NAD<sup>+</sup>/NADH ratio (Murphy, 2009). Compound **30c** significantly reduced the intracellular pools of NAD<sup>+</sup> and NADH by 42.8 % and 57.4 %, respectively (Figure 1.16 A) in 4T1 cells. In contrast, no effect on NAD<sup>+</sup> and NADH pools or NAD<sup>+</sup>/NADH ratio was found in a parallel experiment with H9C2 cells (Figure 1.16 B). Surprisingly, compound **30c** did not decrease NAD<sup>+</sup>/NADH ratio in 4T1 cells but increased it (Figure 1.16 C). Thus, changes in the NAD<sup>+</sup>/NADH ratio are not the ones that induce ROS overproduction.

To determine whether the interaction of the modified isoselenazolium salt **30c** with CL could potentially lead to the observed proton leak and ROS formation, the fluorescence-based competitive binding assay was carried out using mitoplasts isolated from rat liver (Figure 1.16 D).

Although **30c** apparently interacted with CL ( $EC_{50} = 3490 \pm 298 \mu\text{M}$ ), the affinity was approximately 100-fold lower compared to the classic mitotargeting moiety nonyl-TPP bromide ( $EC_{50} = 32.22 \pm 2.64 \mu\text{M}$ ) and approx. 5000-fold lower compared to cyt c ( $EC_{50} = 0.70 \pm 0.14 \mu\text{M}$ ).



**Figure 1.16 NAD<sup>+</sup> and NADH concentrations in (A) 4T1 and (B) H9C2 cells after treatment with 1  $\mu\text{M}$  30c. (C) NAD<sup>+</sup>/NADH ratio in 4T1 and H9C2 cells after treatment with 1  $\mu\text{M}$  30c. (D) Cardiolipin binding curves of cytochrome c (cyt c), nonyltriphenylphosphonium bromide (Nonyl TPP) and 30c in mitoplasts isolated from rat liver\***

\*Values are shown as mean  $\pm$  SD (n = 3–5 experiments). Statistically significant difference (\*) was considered when  $p < 0.05$  (Students *t*-test) compared to the control group.

Therefore, it is unlikely that the interaction of **30c** with CL induces proton leak and decreases the coupling efficiency. Hence, other molecular targets were examined that could be associated with mitochondrial metabolism.

### 1.3.4 Enzymatic screening of isoselenazolium salts

First, PARP inhibitory activity of compound **30c** (0.25  $\mu\text{M}$ ) was examined on 13 PARP family proteins, and it was found that compound **30c** selectively inhibits PARP1 isoform. Looking for other possible molecular

targets, compound **30c** (in 1  $\mu\text{M}$  concentration) was tested on a metabolic enzyme panel, as well as on several members of the Bcl-2 family proteins. Surprisingly, compound **30c** was found to selectively inhibit pyruvate kinase M2 (PKM2), one of the four isoforms of pyruvate kinase that is predominantly expressed in cancer tissues (Israelsen et al., 2013; Liu et al., 2015).

After these intriguing findings, PARP1 and PKM2 inhibitory properties of other isoselenazolium salts were determined (Table 1.5). It turned out that compound **30c** had the highest PARP1 inhibitory activity among studied compounds with  $\text{IC}_{50}$  of  $0.250 \pm 0.08 \mu\text{M}$ , that is approx. 4 times lower than that of compound **3**.

Table 1.5

**$\text{IC}_{50}$  values of isoselenazolium chlorides for PKM2 and PARP1 inhibition and their inhibitory activity on PKM1, PKR and LDH at 1  $\mu\text{M}$  concentration**

Comp.	$\text{IC}_{50}$ , $\mu\text{M}$			Inhibition at 1 $\mu\text{M}$ , %		
	PARP1	PKM2	PKM2 with FBP (250 $\mu\text{M}$ )	PKM1	PKR	LDH
Apigenin	n.t.	> 20	> 20	n.t.	n.t.	n.t.
Comp. 3k (Ning et al., 2017)	n.t.	> 20	> 20	n.t.	n.t.	n.t.
Olaparib	$0.0035 \pm 0.0005$	> 10	> 10	n.t.	n.t.	n.t.
<b>3</b>	$0.970 \pm 0.030$	$2.924 \pm 0.356$	$2.731 \pm 0.277$	n.t.	n.t.	n.t.
<b>30b</b>	$0.359 \pm 0.070$	$0.545 \pm 0.059$	$0.303 \pm 0.081$	$16 \pm 4$	$39 \pm 6$	$10 \pm 3$
<b>30c</b>	$0.250 \pm 0.080$	$0.350 \pm 0.068$	$0.477 \pm 0.104$	$13 \pm 1$	$21 \pm 11$	$10 \pm 7$
<b>30d</b>	$0.769 \pm 0.021$	$0.478 \pm 0.143$	$0.610 \pm 0.022$	$10 \pm 2$	$16 \pm 14$	$13 \pm 4$
<b>30e</b>	$0.307 \pm 0.010$	$0.854 \pm 0.263$	$0.603 \pm 0.023$	$26 \pm 4$	$20 \pm 2$	$7 \pm 2$
<b>30f</b>	$0.322 \pm 0.012$	$0.380 \pm 0.138$	$0.517 \pm 0.036$	$20 \pm 10$	$42 \pm 3$	$6 \pm 2$
<b>30g</b>	$0.438 \pm 0.090$	$0.637 \pm 0.137$	$0.572 \pm 0.021$	$11 \pm 4$	$29 \pm 13$	$2 \pm 1$
<b>30h</b>	> 1	> 1	n.t.	n.t.	n.t.	n.t.
<b>30i</b>	> 1	> 1	n.t.	n.t.	n.t.	n.t.
<b>30j</b>	$0.378 \pm 0.020$	$0.897 \pm 0.385$	n.t.	$29 \pm 1$	$15 \pm 6$	$7 \pm 3$

Table 1.5 continued

Comp.	IC <sub>50</sub> , μM			Inhibition at 1 μM, %		
	PARP1	PKM2	PKM2 with FBP (250 μM)	PKM1	PKR	LDH
30k	> 1	1.355 ± 0.295	n.t.	10 ± 6	28 ± 14	7 ± 2
31b	1.370 ± 0.070	> 1	n.t.	n.t.	n.t.	n.t.
31c	1.620 ± 0.130	1.064 ± 0.266	n.t.	4 ± 3	5 ± 3	9 ± 4
32a	0.275 ± 0.014	> 1	n.t.	n.t.	n.t.	n.t.
32b	0.315 ± 0.080	> 1	n.t.	n.t.	n.t.	n.t.
32c	0.355 ± 0.090	0.420 ± 0.097	0.572±0.103	15 ± 8	37 ± 1	6 ± 2
32d	0.303 ± 0.080	0.362 ± 0.038	0.542±0.030	26 ± 4	40 ± 17	13 ± 5
32e	> 1	1.010 ± 0.264	n.t.	21 ± 3	11 ± 4	6 ± 1
32f	> 1	0.901 ± 0.173	n.t.	23 ± 3	29 ± 10	9 ± 2

\*Values are shown as the means ± SD from at least 3 independent experiments. PKM2, pyruvate kinase M2 isoform; PKM1, pyruvate kinase M1 isoform; PKR, pyruvate kinase R isoform; LDH, L-lactate dehydrogenase; FBP, fructose-1,6-bisphosphate; n.t. – not tested.

PKM2 IC<sub>50</sub> values for the isoselenazolium series were determined by a LDH-coupled assay. Isoselenazolium salts did not inhibit LDH and, therefore, were suitable for the chosen assay. Compounds **30b–32f** were found to selectively inhibit PKM2, and compound **30c** and its amide analogue **32c** stood out with 0.350 ± 0.068 and 0.420 ± 0.097 μM IC<sub>50</sub> values, respectively. Surprisingly, the previously described PKM2 inhibitors apigenin and compound **3k** did not inhibit PKM2 at concentrations up to 20 μM in used conditions. The studied isoselenazolium salts were more selective toward PKM2, as no compound reached a 50 % inhibition of either PKM1 or PKR at a concentration of 1 μM. In particular, the addition of fructose-1,6-bisphosphate (FBP), the natural allosteric activator of PKM2, did not significantly affect the inhibitory activity of the compounds studied.



Importantly, the ester or amide group in the isoselenazolopyridinium ring was essential for PKM2 inhibition, since the previously described unsubstituted isoselenazolopyridinium chloride **3** was approximately 8 times less active than compounds **30c** and **32c**.

### 1.3.5 Pyruvate kinase M2 inhibition mechanisms

The structure-activity relationship (SAR) pattern of the newly discovered PKM2 inhibitors (Figure 1.17 A) corresponded well to that of cytotoxicity. To elucidate the binding and inhibition mechanisms of isoselenazolium salts, the most potent inhibitors **30c** and **32c** were selected for the further biochemical and biophysical studies. To characterise the inhibition mechanism steady-state kinetic parameters for PKM2 for both PEP and ADP were determined in the presence of compound **30c** at different concentrations. It was established that in the presence of compound **30c** the value of  $V_{App,max}$  was constant, while the  $K_{App,M}$  increased at higher inhibitor concentrations for both enzyme substrates. Additionally, a classic competitive inhibitor pattern was revealed in Lineweaver-Burk plots for both substrates (Figures 1.17 B and C).

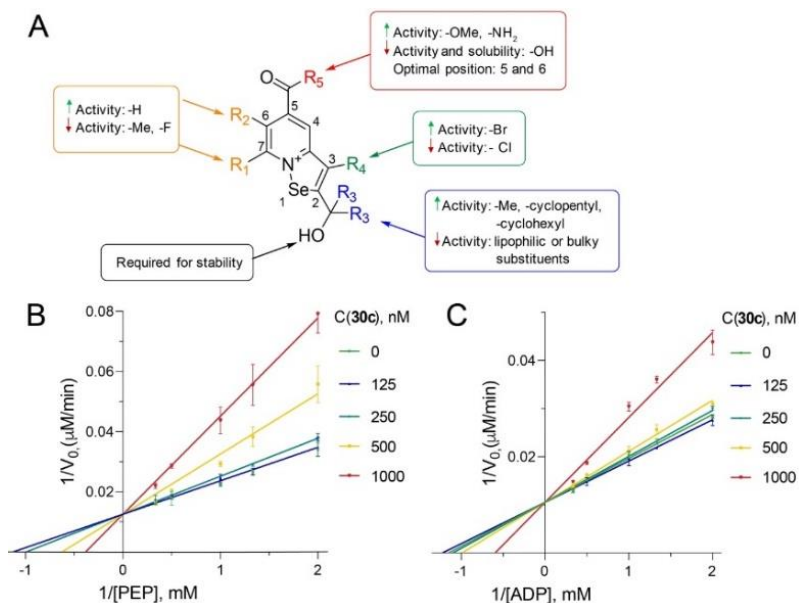


Figure 1.17 **A) Structure-activity relationship for PKM2 inhibitory activity of isoselenazolopyridinium salts; B) PKM2 initial reaction rate ( $V_0$ ) with respect to PEP concentration in the presence of 30c at different concentrations; C) PKM2 initial reaction rate ( $V_0$ ) with respect to ADP concentration in the presence of compound 30c at different concentrations**

The selenium atom in the isoselenazolium moiety has an electrophilic nature and may potentially react covalently with the nucleophilic cysteine side chains on the surface of PKM2. The reversibility of compound **32c** binding was tested using water ligand-observed gradient spectroscopy (WaterLOGSY). Protons of free compound **32c** were observed with negative peak intensities, resulting from the cross relaxation via the nuclear Overhauser effect (NOE) (Figure 1.18 A, bottom). The addition of PKM2 to compound **32c** caused an inversion of the peak intensity, i.e., negative NOE, suggesting that a reversible, noncovalent binding of the ligand to PKM2 has occurred, and the molecule has dissociated during the mixing time of the WaterLOGSY sequence (Figure 1.18 A, top).

PKM2 activity is regulated by a variety of metabolites that affect its quaternary assembly by promoting or inhibiting the more active tetrameric state, or by inducing interprotomer movements that result in altered activity (Wang et al., 2015; Macpherson et al., 2019; Srivastava, Nandi, and Dey, 2019; Nandi and Dey, 2020). To evaluate the effect of isoselenazolium salts on the oligomeric assembly of PKM2, analytical size exclusion chromatography (SEC) measurements were performed. Under the experimental conditions tested, PKM2 eluted from the column primarily as tetrameric species, corresponding to the first peak in the chromatogram, followed by a dimer/monomer peak of a smaller magnitude (Figure 1.18 B). As expected, the ratio of tetramer to dimer/monomer increased at higher protein concentrations. Incubation of 5  $\mu$ M PKM2 with compound **30c** or **32c** resulted in a dose-dependent increase in the tetramer ratio, with a concurrent reduction in the dimer/monomer peak (Figure 1.18 C).

However, SEC required a micromolar concentration of a protein, and the observed PKM2 dimer/tetramer ratio could not be physiologically relevant, considering its strong dependence on the concentration. Therefore, it was decided to apply single-molecule mass photometry to explore the oligomeric state of PKM2 at lower concentration. At a concentration of 50 nM (Figure 1.18 D) PKM2 was mostly in the dimeric state ( $69.1 \pm 1.9$  % of total oligomers), while monomers and tetramers were less prevalent ( $11.1 \pm 3.0$  % and  $19.8 \pm 4.3$  %, respectively).

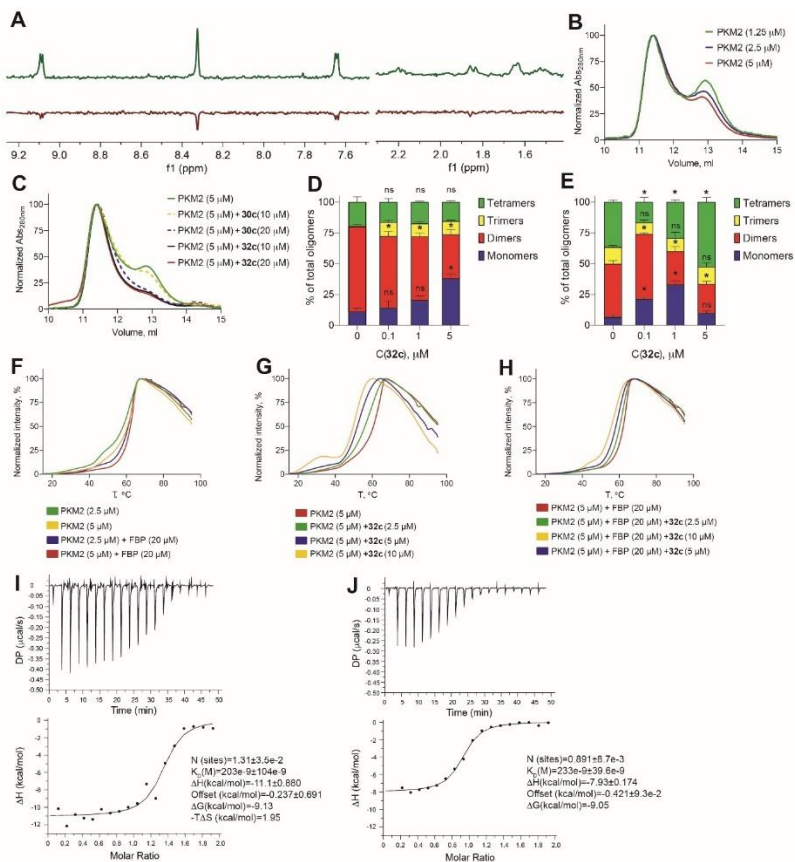
As in the SEC experiment, the addition of compound **32c** led to a decrease in the dimer population in a dose-dependent manner, and at 5  $\mu$ M two-fold reduction was observed ( $69.1 \pm 1.9$  % vs  $35.8 \pm 4.0$  %,  $p < 0.0001$ ). At the same time, the percentage of monomers was increased only at 5  $\mu$ M (up to  $38.0 \pm 3.8$  %,  $p = 0.0002$ ). Interestingly, formation of trimeric species with molecular mass of approx. 180 kDa, that could not be distinguished by the SEC, could be clearly observed in mass photometry histograms. As expected, the

addition of FBP (100  $\mu\text{M}$ ) increased the amount of tetramer and trimer at the expense of the dimer (Figure 1.18 E).

When both FBP and compound **32c** were added, the changes in the populations became more complex, (Figure 1.14 E) however, at 5  $\mu\text{M}$  concentration, there was also an almost two-fold reduction in the amount of dimer ( $43.2 \pm 2.5\%$  vs  $23.7 \pm 1.8\%$ ,  $p < 0.0001$ ), but in this case there was an increase in the proportion of tetrameric species ( $36.6 \pm 1.5\%$  vs  $52.6 \pm 3.7\%$ ,  $p = 0.0004$ ). The results of both SEC and mass photometry are in stark contrast to previously published observations that natural activators of PKM2, such as FBP and serine, promote the formation of tetramers, while PKM2 inhibitors increase the proportion of dimeric/monomeric species (Nandi and Dey, 2020).

The melting temperature of PKM2 was examined using a SYPRO Orange-based differential scanning fluorimetry (DSF) assay. The PKM2 melting curves displayed a multimodal character (Figure 1.18 F). The decrease in PKM2 concentration from 5 to 2.5  $\mu\text{M}$  led to an increase in low-stability species. For 2.5  $\mu\text{M}$  PKM2, three distinct transitions were observed: the first in 20–40  $^{\circ}\text{C}$  range, followed by 40–50  $^{\circ}\text{C}$ , and finally a dominant transition at 60  $^{\circ}\text{C}$ . These data suggest that a mixture of species of different stabilities exist that, presumably, represent distinct oligomeric states. Alternatively, the observed species may represent different conformational states in the oligomeric assembly, such as the previously reported T- or R-states (Wang et al., 2015).

FBP has been shown to stabilise PKM2 against thermal denaturation, and the data obtained was in a good agreement with previously published report and consistent with the mass photometry measurements (Wang et al., 2015). FBP decreased the population of low-stability species but did not change the temperature at which maximum fluorescence is obtained, suggesting that FBP induced the formation of high-stability species but did not significantly stabilise the tertiary fold.



**Figure 1.18 A) WaterLOGSY spectra of 250  $\mu\text{M}$  32c alone (bottom, red) or in the presence of 12.5  $\mu\text{M}$  PKM2 (top, green); B) SEC of PKM2 at various concentrations; C) SEC of PKM2 preincubated with 30c or 32c; D) Oligomeric state of PKM2 in the presence of 32c revealed by mass photometry; E) Oligomeric state of PKM2 in the presence of FBP and 32c at different concentrations revealed by mass photometry; F) DSF thermal melt data for PKM2 alone or in the presence of FBP; G) DSF thermal melt data for PKM2 in the presence of 32c; H) DSF thermal melt data for PKM2 in the presence of FBP and 32c; I) Isotherm of PKM2 titration with FBP; J) Isotherm of PKM2 titration with FBP after preincubation with 32c \***

\*The results are presented as a mean value of at least 3 independent experiments. Statistically significant difference (\*) was considered when  $p < 0.05$  (one-way ANOVA) compared to the control group.

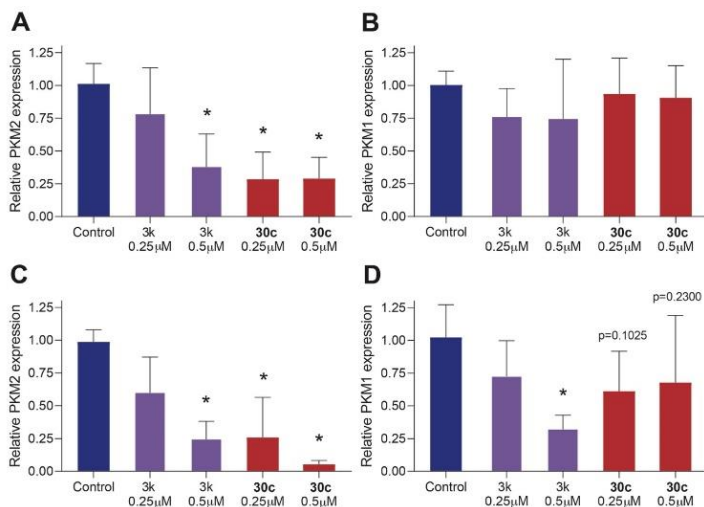
Compound **32c** destabilised PKM2 in a dose-dependent manner (Figure 1.18 G). Destabilisation may arise as a result of a change in the oligomeric assembly or as a result of changes in the tertiary fold. At high concentration (10  $\mu\text{M}$ ), compound **32c** induced the formation of a significantly destabilised population which melts at 20–40  $^{\circ}\text{C}$ , that is only marginally present for PKM2 alone. In turn, FBP decreased the magnitude of destabilisation induced by compound **32c** (Figure 1.18 H). Because FBP does not appear to stabilise the tertiary, but rather the quaternary structure, it is possible that compound **32c** and FBP induce competing conformational changes in the PKM2 oligomer. This suggestion is in line with the ITC data, which showed that FBP had a high affinity for PKM2 in the absence (Figure 1.18 I) and in the presence of compound **32c** (Figure 1.18 J) but had a substantially lower binding enthalpy in the latter case, suggesting that the local interactions of FBP with the enzyme are maintained, while its effect on the quaternary structure is perturbed.

### **1.3.6 Alterations in mRNA expression of pyruvate kinases M2 and M1**

Another way to modulate enzyme activity is to reduce its expression. The expression of PKM1 and PKM2 mRNA was evaluated by qPCR, and compound **3k** was used as a positive control. Treatment of 4T1 cells with compound **30c** (0.25 and 0.5  $\mu\text{M}$ ) for 24 h resulted in an approximately three-fold decrease in the expression of PKM2 mRNA compared to untreated cells ( $p < 0.001$ ), while the expression of PKM1 was not significantly altered (Figure 1.19 A and B, respectively). Although compound **3k** was not active in the enzymatic assay, it was able to reduce the expression of PKM2 mRNA in 4T1 cells at 0.5  $\mu\text{M}$ .

In case of HCC1937, treatment with 0.25 and 0.5  $\mu\text{M}$  compound **30c** caused a 4-fold and 20-fold decrease in the expression of PKM2, respectively (Figure 1.19 C), while **3k** was effective only at 0.5  $\mu\text{M}$ . At the same time, PKM1

expression was not statistically significantly reduced by compound **30c** (Figure 1.19 D); however, compound **3k** induced a three-fold decrease in PKM1 mRNA levels ( $p = 0.0021$ ). Therefore, compound **30c** modulated the expression of PKM2 mRNA more effectively and selectively than compound **3k** in both studied cell lines.



**Figure 1.19 Relative PKM2 mRNA expression in 4T1(A) and HCC1937 (C) cells and relative PKM1 mRNA expression in 4T1(B) and HCC1937 (D) cells obtained by qPCR after 24h treatment with compound 3k or 30c at 0.25 and 0.5 μM concentrations\***

\* The results are presented as mean  $\pm$  SD of 5–7 independent experiments. Statistically significant difference (\*) was considered when  $p < 0.05$  (one-way ANOVA) compared to the control group (vehicle).

### 1.3.7 Prevention of pyruvate kinase M2 nuclear translocation

Apart from its role in glycolysis, dimeric form of PKM2 can translocate into the nucleus where it functions as protein kinase and a transcriptional coactivator of many genes associated with carcinogenesis (Zahra et al., 2020). Furthermore, it has been reported that among numerous post-translational

modifications PKM2 can undergo PARylation (modification with poly(ADP-ribose), PAR) in a nucleus catalysed by PARP1. PARylation enhances nuclear retention of PKM2 and is required for proto-oncogene c-Myc and glycolysis-related GLUT and LDH genes induction (Li et al., 2016). Considering isoselenazolium salts PARP1 inhibitory activity and ability to reduce dimer amount of PKM2, it was of special interest to investigate whether they can impede nuclear translocation of PKM2.

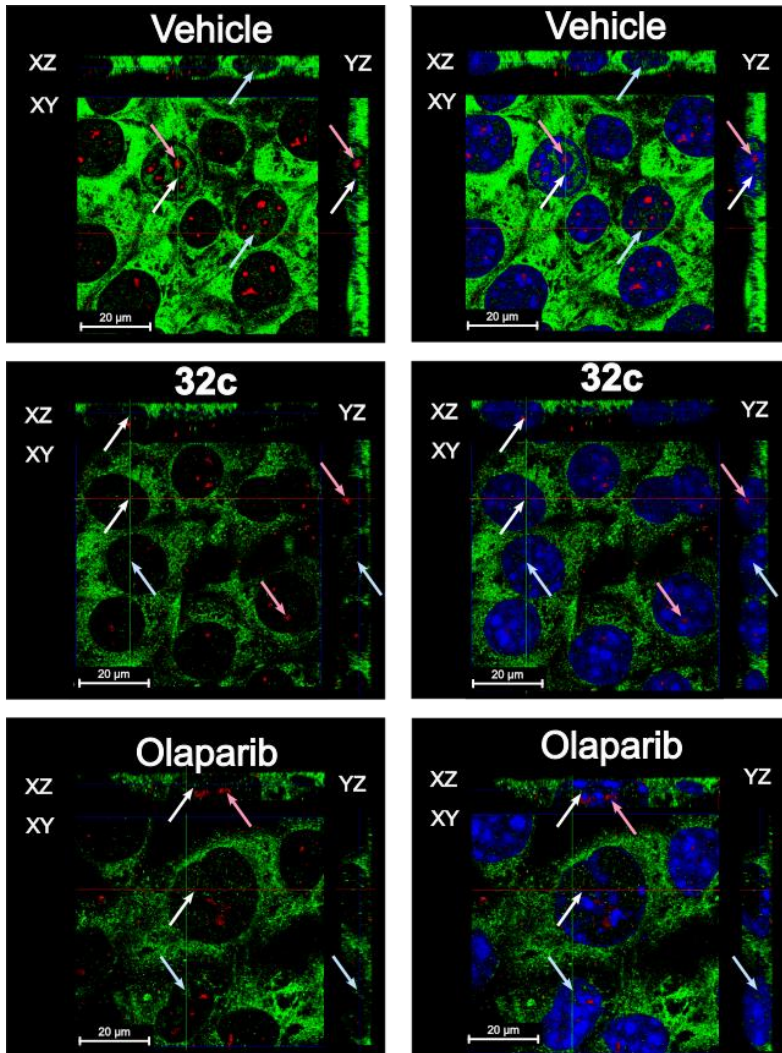
Intracellular localisation of PKM2 and PAR in 4T1 cells was examined by double immunofluorescence labelling with subsequent analysis by confocal microscopy (Figure 1.20).

In the control group (vehicle), the PKM2 signal was high all across the cytoplasm, however nuclear location of PKM2 was indisputably confirmed in the XZ and YZ sections by counterstaining the nuclei with DAPI. After treatment of the cells with compound **32c**, as anticipated from the qPCR data, PKM2 signal throughout the cells was lower, and, surprisingly, treatment with olaparib gave similar results.

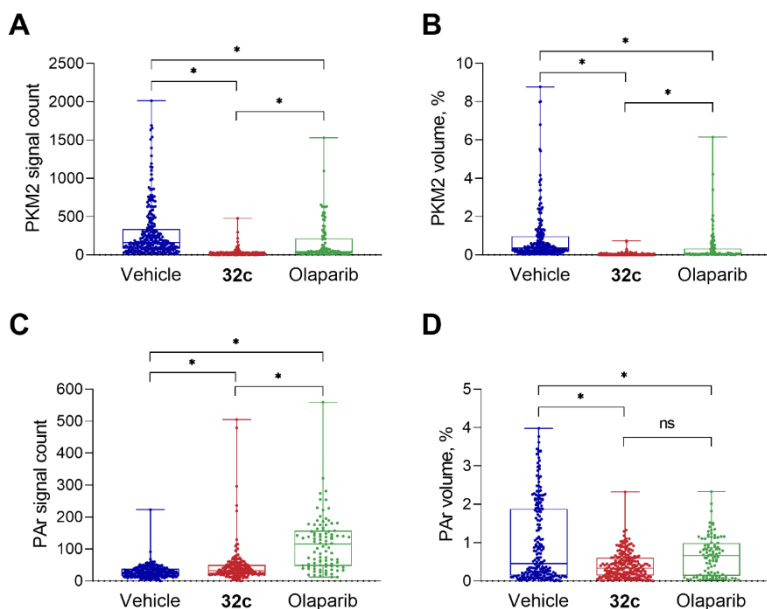
To quantitatively assess nuclear translocation of PKM2 and the amount of PAR, signal counts inside the nuclei and relative volume occupied were analysed. The analysis revealed that both compound **32c** and olaparib significantly decreased the PKM2 signal count (Figure 1.21 A) and the relative volume (Figure 1.21 B) compared to the control cells, and a pairwise comparison using Dunn's test showed that compound **32c** was superior to olaparib ( $p < 0.001$ ) in both aspects.

Unlike PKM2, that mainly generates a point signal, PAR forms long polymer chains that are seen on image as large aggregates. PAR count inside the nuclei after compound **32c** or olaparib (Figure 1.21 C) was higher than in the control group ( $p < 0.001$ ), but the relative volume taken by these aggregates (Figure 1.21 D) was smaller ( $p < 0.001$ ).





**Figure 1.20 Representative confocal images of PKM2 (green) and PAR (red) localisation in 4T1 cells in orthogonal projections after treatment with vehicle (control, upper section), 32c (2 µM, middle section) or olaparib (2 µM, lower section) followed by stimulation with CoCl<sub>2</sub> (100 µM). Nuclei were counterstained with DAPI (blue)**



**Figure 1.21 A) PKM2 signal count inside the nuclei; B) Relative volume of nuclei taken by PKM2; C) PAR signal count inside the nuclei; D) Relative volume of nuclei taken by PAR after 24 h treatment of 4T1 cells with vehicle, 32c or olaparib (2  $\mu$ M) with subsequent stimulation with CoCl<sub>2</sub> (100  $\mu$ M) for 24h\***

\*Each point represents a single cell. Data was analysed with Kruskal-Wallis test followed by Dunn's multiple comparisons test. Statistically significant difference (\*) was considered when  $p < 0.05$ .

Thus, shorter PAR chains were formed that confirmed inhibition of PARP activity. The effects of compound **32c** and olaparib were similar, although PAR count after compound **32c** treatment was slightly lower than after olaparib, while no difference between reduction in relative volume was observed between the two. Therefore, isoselenazolium salts reduce PKM2 amount in the nuclei, presumably, by decreasing the amount of PKM2 dimers and preventing its nuclear retention by inhibition of PARP1.

## 2 Discussion

The discovery of a mechanism of action is a corner stone in the development of new drug candidates for anticancer therapy. The first generation of isoselenazolium salts had high cytotoxicity against breast cancer *in vitro* and was much less cytotoxic to normal cells. As expected, these selenium-containing compounds affected cellular metabolism: reduced NAD<sup>+</sup> and NADH levels, inhibited PARP1, pyruvate-dependent mitochondrial respiration, and induced ROS production. It was clear, that isoselenazolium salts compromise mitochondrial CI output, but do not directly inhibit CI, however, the precise mechanism of action was not identified first. As CI is stabilised by CL, its activity can be affected by ROS-induced peroxidation of CL or by destabilisation of lipid bilayer through a direct interaction (Paradies et al., 2002; Petrosillo et al., 2007). NMR and ITC data suggested that isoselenazolium salts interacted with CL and it was initially proposed as a potential molecular target.

Traditional drug targets, e.g. enzymes, receptors and ion channels usually have robust screening assays that are suitable for high throughput screening. Historically, particular phospholipids, such as CL, were recognised as a prospective drug target much later and until now there were no available drug screening methods. Therefore, a new CL-specific fluorescent probe was developed for a competitive binding assay. The new screening assay allows to assess CL as a potential molecular target and would be highly appreciated by scientists working on therapies designed to protect or damage the inner mitochondrial membrane, targeted drug delivery into mitochondria, or antimicrobial therapy. Additionally, this method might help predict drug interactions with the mitochondrial membrane and, perhaps, warn about possible side effects related to mitochondrial dysfunction in the early stage of a research. However, the isoselenazolium salts in this assay showed a low affinity for CL; therefore, their cytotoxic effect can hardly be attributed to the direct interaction

with CL. These results underscore the importance of using various methods based on different principles to validate a molecular target.

The second generation of isoselenazolium derivatives exhibited high cytotoxic effect not only against breast cancer, but also against hepatocellular carcinoma, lung cancer and T cell leukaemia models *in vitro*. These compounds were more potent PARP1 inhibitors, however, showed similar effect on mitochondrial respiration as the first-generation compounds. Consequently, it was found that compound **30c** is a potent and selective PKM2 inhibitor.

Understanding the precise molecular mechanism of the interaction of a ligand with a target protein is crucial for hit-to-lead optimisation. Atomic-level structural methods, such as protein X-ray crystallography, provide the most detailed insight for target-based drug design, however, attempts to obtain PKM2 and isoselenazolium salts co-crystals were unsuccessful. Apparently, co-crystallisation was obstructed by the destabilisation of the quaternary structure by the compounds. Therefore, other biochemical and biophysical methods had to be used to explore the binding mechanism. Although isoselenazolium salts have a kinetic signature of a competitive inhibitor, it does not necessarily mean that they unequivocally bind to the active site of the enzyme. An inhibitor and a substrate could bind to different sites that negatively interfere with one another, that is, through allosteric interactions driven by inhibitor-induced conformational changes (Robert A. Copeland, 2013). This is a rare occasion, but such competitive allosteric inhibition mechanism has been reported a few times (Luo et al., 2007; Alphey et al., 2013; Feldman et al., 2016). DSF, SEC and mass photometry data indicate that isoselenazolium salts inhibit PKM2 in a noncanonical fashion, inducing an unstable, functionally deficient tetrameric conformation. Notably, a natural PKM2 allosteric activator FBP does not compete with isoselenazolium salts binding site nor restore enzymatic function

and quaternary structure at physiologically relevant concentration (Macpherson et al., 2019).

The proposed isoselenazolium's mechanism of action is schematically shown in Figure 2.1. As PKM2 is the only enzyme producing ATP in the energy payoff phase of glycolysis, inhibition of PKM2 enzymatic function makes the main ATP production pathway in cancer cells unprofitable. At the same time, CI and OXPHOS coupling are disrupted, presumably by a drastic increase in ROS production, that should furthermore exacerbate the cellular energy crisis.

Although it has been shown that PKM2 in its inactive dimeric state stimulates ROS detoxification by increasing glucose-6-phosphate flux into the pentose phosphate pathway, which provides NADPH for glutathione reductase (Anastasiou et al., 2011), and inhibits ROS-induced apoptosis by phosphorylating and stabilising Bcl-2 (Liang et al., 2017), it does not cope with isoselenazolium-induced oxidative burst. Concurrently, overall PKM2 expression is also substantially reduced. Additionally, it was found that compound **30c** significantly decreased NAD<sup>+</sup> and NADH pools in breast cancer cells and had no effect in cardiomyoblasts. Whether it is a consequence of inhibition of PKM2 or an off-target effect remains to be discovered.

As previously reported, the dimeric form of PKM2 translocates to the nucleus, where it acts as a protein kinase and a transcriptional coactivator, while the tetrameric form does not (Dong et al., 2016). Therefore, a decrease in the amount of dimeric species is crucial for the suppression of PKM2 nonmetabolic function and the suppression of the tumour growth. For example, Gao and colleagues has shown that a mutant PKM2 (R399E), which does not form a tetramer, promotes STAT3 phosphorylation and increases tumour growth rate *in vivo* compared to the wild-type PKM2-expressing tumour in a colon adenocarcinoma model (Gao et al., 2012).

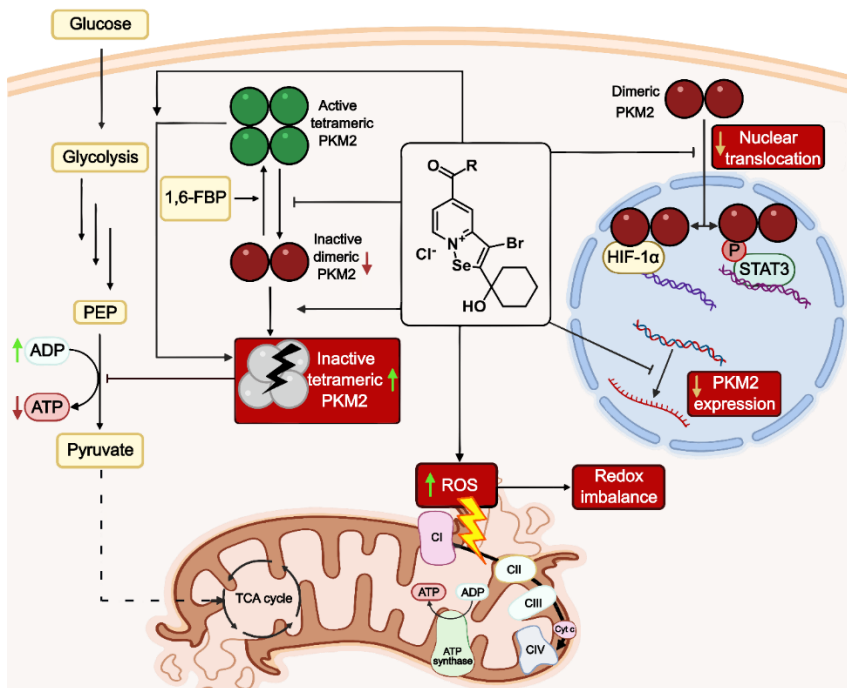


Figure 2.1 **Proposed mechanism of action of isoselenazolium salts**

In this work it was found that compound **32c** decreases the presence of PKM2 in the nuclei and there are two mechanisms involved. Firstly, the dimer amount of PKM2 that can move into the nuclei is lowered, and secondly, PARylation of PKM2 by PARP1 is inhibited and nuclear retention is impaired.

Thereby, isoselenazolium salts restrain PKM2 functions at three levels: decrease protein expression, reduce metabolic enzymatic function, and prevent nuclear non-metabolic functions by the restriction of translocation. It is yet unknown which of these effects contributes the most to the antiproliferative activity, but it can be speculated that the decrease in the dimer/tetramer ratio is the most important. Such assumption has been supported by the similar antiproliferative activity of small molecule PKM2 activators that promote active

tetramer formation, reduce dimer amount, and block nuclear translocation (Warner, Carpenter, and Bearss, 2014; Giannoni et al., 2015; Li et al., 2018).

An open question is how isoselenazolium salts cause such an increase in mitochondrial ROS production. The results demonstrated that ROS overproduction is not caused by the decrease of the  $\text{NAD}^+/\text{NADH}$  ratio nor the reverse electron transport. What is noticeable is that PKM2 has also been reported to be involved in mitochondrial ROS generation, although the precise mechanism is unknown (Gao et al., 2022). Inversely, PKM2 activators TEPP-46 and DASA-58 were shown to reduce ROS production. Thus, these results suggest the possible relationship between PKM2 inhibition and ROS overproduction. However, it is possible that isoselenazolium salts affect glutathione levels or its metabolism, but further studies are needed to verify this.

Taken together, these findings establish a ground for the novel class of drug candidates with a unique molecular mechanism and reveal specific structural features of PKM2. Furthermore, a potent and stable inhibitor would be an integral part of future studies focusing on the metabolic role of PKM2 in cancer.

## Conclusions

1. The hypothesis was confirmed: isoselenazolium derivatives exhibit high cytotoxicity in breast, liver, lung, and T-cell leukaemia cell models. These compounds have a wide impact on energy metabolism in cancer cells, including modulation of pyruvate-dependent mitochondrial respiration, induction of H<sub>2</sub>O<sub>2</sub> production, dyscoupling of the electron transport system, decrease in NAD<sup>+</sup> concentration, inhibition of PARP1 and PKM2.
2. The competitive binding assay based on the cardiolipin-specific fluorescent probe **20** offers a robust way to determine relative affinity for cardiolipin. However, isoselenazolium salts affinity is low and is unlikely to be associated with its pharmacological activity.
3. An ester or amide group in the position 5 or 6 of the isoselenazolopyridinium ring is essential for both PARP1 and PKM2 inhibitory activity.
4. The major molecular target for isoselenazolium salts is PKM2. Isoselenazolium chlorides have an unusual mechanism of PKM2 inhibition, inducing a functionally deficient tetrameric assembly that leads to impaired enzymatic function and decreased nuclear transfer.



## List of publications, reports and patents on the topic of the Thesis

### Publications

1. **Dimitrijevs, P.**, Domracheva, I., Arsenyan, P. 2020. Improved method for the preparation of nonyl acridine orange analogues and utilization in detection of cardiolipin. *New Journal of Chemistry*. 44(23), 9626–9633. doi:10.1039/D0NJ02116D
2. Makrecka-Kuka, M., **Dimitrijevs, P.**, Domracheva, I., Jaudzems, K., Dambrova, M., Arsenyan, P. 2020. Fused isoselenazolium salts suppress breast cancer cell growth by dramatic increase in pyruvate-dependent mitochondrial ROS production. *Scientific Reports*. 10(1), 21595. doi:10.1038/s41598-020-78620-8
3. **Dimitrijevs, P.**, Arsenyan, P. 2021. Cardiolipin in the spotlight: Quantitative analysis and fluorescence-based competitive binding assay. *Sensors and Actuators B: Chemical*. 346, 130537. doi:10.1016/j.snb.2021.130537
4. **Dimitrijevs, P.**, Makrecka-Kuka, M., Bogucka, A., Hyvönen, M., Pantelejevs, T., Arsenyan, P. 2023. Development of isoselenazolium chlorides as selective pyruvate kinase isoform M2 inhibitors. *European Journal of Medicinal Chemistry*. 257, 115504. doi:10.1016/j.ejmech.2023.115504

### Reports and theses at international congresses and conferences

1. **Dimitrijevs, P.** Novel method for evaluating cardiolipin as a potential molecular drug target and its quantitative analysis, 12th World Congress on Targeting Mitochondria, October 27-29, 2021, online.

### Patent applications

1. Arsenjans, P., **Dimitrijevs, P.** Fluorescent acridinium salts, synthesis thereof and use for detection of cardiolipin. WO2021105780A1, 2021.
2. Arsenjans, P., **Dimitrijevs, P.** An assay for measuring binding affinity for cardiolipin of biologically active compounds. WO2022038424A1, 2022.
3. Arsenjans, P., **Dimitrijevs, P.**, Makrecka-Kuka, M. Novel pyruvate kinase isoform M2 inhibitors. Filed: 20.04.2022, (LVP2022000034).

## References

1. Alphey, M. S., Pirrie, L., Torrie, L. S., Boulkeroua, W. A., Gardiner, M., Sarkar, A., Maringer, M., Oehlmann, W., Brenk, R., Scherman, M. S., Mcneil, M., Rejzek, M., Field, R. A., Singh, M., Gray, D., Westwood, N. J., Naismith, J. H. 2013. Allosteric Competitive Inhibitors of the Glucose-1-phosphate Thymidyltransferase (RmlA) from *Pseudomonas aeruginosa*. *ACS Chemical Biology*. 8, 387–397.
2. Anastasiou, D., Pouligiannis, G., Asara, J. M., Boxer, M. B., Jiang, J. kang, Shen, M., Bellinger, G., Sasaki, A. T., Locasale, J. W., Auld, D. S., Thomas, C. J., Heiden, M. G. Vander, Lewis, C. 2011. Inhibition of pyruvate kinase M2 by reactive oxygen species contributes to cellular antioxidant responses. *Science*. 334(6060), 1278–1283. doi:10.1126/science.1211485. Inhibition
3. Arsenyan, P., Vasiljeva, J., Belyakov, S., Liepinsh, E., Petrova, M. 2015. Fused Selenazolinium Salt Derivatives with a Se-N<sup>+</sup> Bond: Preparation and Properties. *European Journal of Organic Chemistry*. 2015(26), 5842–5855. doi:10.1002/ejoc.201500582
4. Chen, Z., Tan, L., Hu, L., Luan, Y. 2015. Superior fluorescent probe for detection of potassium ion. *Talanta*. 144, 247–251. doi:10.1016/j.talanta.2015.06.015
5. Chuai, H., Zhang, S. Q., Bai, H., Li, J., Wang, Y., Sun, J., Wen, E., Zhang, J., Xin, M. 2021. Small molecule selenium-containing compounds: Recent development and therapeutic applications. *European Journal of Medicinal Chemistry*. 223, 113621. doi:10.1016/j.ejmech.2021.113621
6. Dong, G., Mao, Q., Xia, W., Xu, Y., Wang, J., Xu, L., Jiang, F. 2016. PKM2 and cancer: The function of PKM2 beyond glycolysis. *Oncology Letters*. 11(3), 1980–1986. doi:10.3892/ol.2016.4168
7. Fan, J., Kamphorst, J. J., Mathew, R., Chung, M. K., White, E., Shlomi, T., Rabinowitz, J. D. 2013. Glutamine-driven oxidative phosphorylation is a major ATP source in transformed mammalian cells in both normoxia and hypoxia. *Molecular Systems Biology*. 9(712), 1–11. doi:10.1038/msb.2013.65
8. Feldman, H. C., Tong, M., Wang, L., Meza-acevedo, R., Gobillot, T., Lebedev, I., Hari, S. B., Gliedt, M. J., Arinjay, K., Backes, B. J., Papa, F. R., Seeliger, M. A., Maly, D. J. 2016. Structural and Functional Analysis of the Allosteric Inhibition of IRE1 $\alpha$  with ATP-Competitive Kinase Ligands Structural and Functional Analysis of the Allosteric Inhibition of IRE1 $\alpha$  with ATP-Competitive Ligands. *ACS Chemical Biology*. 11(8), 2195–2205. doi:10.1021/acschembio.5b00940
9. Forman, H. J., Azzi, A. 1997. On the virtual existence of superoxide anions in mitochondria: thoughts regarding its role in pathophysiology. *The FASEB Journal*. 11(5), 374–375. doi:10.1096/fasebj.11.5.9141504

10. Gandin, V., Khalkar, P., Braude, J., Fernandes, A. P. 2018. Organic selenium compounds as potential chemotherapeutic agents for improved cancer treatment. *Free Radical Biology and Medicine*. 127, 80–97. doi:10.1016/j.freeradbiomed.2018.05.001
11. Gao, J., Zhao, Y., Li, T., Gan, X., Yu, H. 2022. The Role of PKM2 in the Regulation of Mitochondrial Function: Focus on Mitochondrial Metabolism, Oxidative Stress, Dynamic, and Apoptosis. *Oxidative Medicine and Cellular Longevity*. 2022.
12. Gao, X., Wang, H., Yang, J. J., Liu, X., Liu, Z. R. 2012. Pyruvate Kinase M2 Regulates Gene Transcription by Acting as a Protein Kinase. *Molecular Cell*. 45(5), 598–609. doi:10.1016/j.molcel.2012.01.001
13. Garbo, S., Di Giacomo, S., Łażewska, D., Honkisz-Orzechowska, E., Di Sotto, A., Fioravanti, R., Zwergel, C., Battistelli, C. 2022. Selenium-Containing Agents Acting on Cancer – A New Hope? *Pharmaceutics*. 15(1), 104. doi:10.3390/pharmaceutics15010104
14. Giannoni, E., Taddei, M. L., Morandi, A., Comito, G., Calvani, M., Bianchini, F., Richichi, B., Raugei, G., Wong, N., Tang, D., Chiarugi, P. 2015. Targeting stromal-induced pyruvate kinase M2 nuclear translocation impairs OXPHOS and prostate cancer metastatic spread. *Oncotarget*. 6(27), 24061–24074. doi:10.18632/oncotarget.4448
15. Gorrini, C., Harris, I. S., Mak, T. W. 2013. Modulation of oxidative stress as an anticancer strategy. *Nature Reviews Drug Discovery*. 12(12), 931–947. doi:10.1038/nrd4002
16. Grevengoed, T. J., Martin, S. A., Katunga, L., Cooper, D. E., Anderson, E. J., Murphy, R. C., Coleman, R. A. 2015. Acyl-CoA synthetase 1 deficiency alters cardiolipin species and impairs mitochondrial function. *Journal of Lipid Research*. 56(8), 1572–1582. doi:10.1194/jlr.M059717
17. Grimm, J. B., English, B. P., Chen, J., Slaughter, J. P., Zhang, Z., Revyakin, A., Patel, R., Macklin, J. J., Normanno, D., Singer, R. H., Lionnet, T., Lavis, L. D. 2015. A general method to improve fluorophores for live-cell and single-molecule microscopy. *Nature Methods*. 12(3), 244–250. doi:10.1038/nmeth.3256
18. Houtkooper, R. H., Cantó, C., Wanders, R. J., Auwerx, J. 2010. The secret life of NAD<sup>+</sup>: An old metabolite controlling new metabolic signaling pathways. *Endocrine Reviews*. 31(2), 194–223. doi:10.1210/er.2009-0026
19. Israelsen, W. J., Dayton, T. L., Davidson, S. M., Fiske, B. P., Hosios, A. M., Bellinger, G., Li, J., Yu, Y., Sasaki, M., Horner, J. W., Burga, L. N., Xie, J., Jurczak, M. J., Depinho, R. A., Clish, C. B., Jacks, T., Kibbey, R. G., Wulf, G. M., Di Vizio, D., Mills, G. B., Cantley, L. C., Vander Heiden, M. G. 2013. PKM2 isoform-specific deletion reveals a differential requirement for pyruvate kinase in tumor cells. *Cell*. 155(2), 397. doi:10.1016/j.cell.2013.09.025

20. Johnson, W. D., Morrissey, R. L., Kapetanovic, I., Crowell, J. A., McCormick, D. L. 2008. Subchronic oral toxicity studies of Se-methylselenocysteine, an organoselenium compound for breast cancer prevention. *Food and Chemical Toxicology*. 46(3), 1068–1078. doi:10.1016/j.fct.2007.11.001
21. Katsyuba, E., Romani, M., Hofer, D., Auwerx, J. 2020. NAD<sup>+</sup> homeostasis in health and disease. *Nature Metabolism*. 2(1), 9–31. doi:10.1038/s42255-019-0161-5
22. Kiebish, M. A., Han, X., Cheng, H., Seyfried, T. N. 2009. *In Vitro* Growth Environment Produces Lipidomic and Electron Transport Chain Abnormalities in Mitochondria from Non-Tumorigenic Astrocytes and Brain Tumours. *ASN Neuro*. 1(3), AN20090011. doi:10.1042/AN20090011
23. Kim, C. W., Choi, K. C. 2021. Effects of anticancer drugs on the cardiac mitochondrial toxicity and their underlying mechanisms for novel cardiac protective strategies. *Life Sciences*. 277(February), 119607. doi:10.1016/j.lfs.2021.119607
24. Kuznetsov, A. V., Javadov, S., Sickinger, S., Frotschnig, S., Grimm, M. 2015. H9c2 and HL-1 cells demonstrate distinct features of energy metabolism, mitochondrial function and sensitivity to hypoxia-reoxygenation. *Biochimica et Biophysica Acta – Molecular Cell Research*. 1853(2), 276–284. doi:10.1016/j.bbamcr.2014.11.015
25. Lenardão, E. J., Sancineto, L., Santi, C. 2018. *New Frontiers in Organoselenium Compounds* 1st ed. 2018. Cham : Springer International Publishing : Imprint: Springer. doi:10.1007/978-3-319-92405-2
26. Li, J., Li, S., Guo, J., Li, Q., Long, J., Ma, C., Ding, Y., Yan, C., Li, L., Wu, Z., Zhu, H., Li, K. K., Wen, L., Zhang, Q., Xue, Q., Zhao, C., Liu, N., Ivanov, I., Luo, M., Xi, R., Long, H., Wang, P. G., Chen, Y. 2018. Natural Product Micheliolide (MCL) Irreversibly Activates Pyruvate Kinase M2 and Suppresses Leukemia. *Journal of Medicinal Chemistry*. 61(9), 4155–4164. doi:10.1021/acs.jmedchem.8b00241
27. Li, N., Feng, L., Liu, H., Wang, J., Kasembeli, M., Tran, M. K., Tweardy, D. J., Lin, S. H., Chen, J. 2016. PARP Inhibition Suppresses Growth of EGFR-Mutant Cancers by Targeting Nuclear PKM2. *Cell Reports*. 15(4), 843–856. doi:10.1016/j.celrep.2016.03.070
28. Liang, J., Cao, R., Wang, X., Zhang, Y., Wang, P., Gao, H., Li, C. 2017. Mitochondrial PKM2 regulates oxidative stress-induced apoptosis by stabilizing Bcl2. *Cell Research*. 27, 329–351. doi:10.1038/cr.2016.159
29. Liu, W. R., Tian, M. X., Yang, L. X., Lin, Y. L., Jin, L., Ding, Z. Bin, Shen, Y. H., Peng, Y. F., Gao, D. M., Zhou, J., Qiu, S. J., Dai, Z., He, R., Fan, J., Shi, Y. H. 2015. PKM2 promotes metastasis by recruiting myeloid-derived suppressor cells and indicates poor prognosis for hepatocellular carcinoma. *Oncotarget*. 6(2), 846–861. doi:10.18632/oncotarget.2749

30. Luo, L., Parrish, C. A., Nevins, N., McNulty, D. E., Chaudhari, A. M., Carson, J. D., Sudakin, V., Shaw, A. N., Lehr, R., Zhao, H., Sweitzer, S., Lad, L., Wood, K. W., Sakowicz, R., Annan, R. S., Huang, P. S., Jackson, J. R., Dhanak, D., Copeland, R. A., Auger, K. R. 2007. ATP-competitive inhibitors of the mitotic kinesin KSP that function via an allosteric mechanism. *Nature Chemical Biology*. 3(11), 722–726. doi:10.1038/nchembio.2007.34
31. Macpherson, J. A., Theisen, A., Masino, L., Fets, L., Driscoll, P. C., Encheva, V., Snijders, A. P., Martin, S. R., Kleinjung, J., Barran, P. E., Fraternali, F., Anastasiou, D. 2019. Functional cross-talk between allosteric effects of activating and inhibiting ligands underlies PKM2 regulation. *eLife*. 8, 1–36. doi:10.7554/eLife.45068
32. Mileykovskaya, E., Dowhan, W., Birke, R. L., Zheng, D., Lutterodt, L., Haines, T. H. 2001. Cardiolipin binds nonyl acridine orange by aggregating the dye at exposed hydrophobic domains on bilayer surfaces. *FEBS Letters*. 507(2), 187–190. doi:10.1016/S0014-5793(01)02948-9
33. Murphy, M. P. 2009. How mitochondria produce reactive oxygen species. *Biochemical Journal*. 417(1), 1–13. doi:10.1042/BJ20081386
34. Nandi, S., Dey, M. 2020. Biochemical and structural insights into how amino acids regulate pyruvate kinase muscle isoform 2. *Journal of Biological Chemistry*. 295(16), 5390–5403. doi:10.1074/jbc.RA120.013030
35. Ning, X., Qi, H., Li, R., Li, Y., Jin, Y. 2017. Discovery of novel naphthoquinone derivatives as inhibitors of the tumor cell specific M2 isoform of pyruvate kinase. *European Journal of Medicinal Chemistry*. 138, 343–352. doi:10.1016/j.ejmech.2017.06.064
36. Paradies, G., Paradies, V., Ruggiero, F. M., Petrosillo, G. 2019. Role of Cardiolipin in Mitochondrial Function and Dynamics in Health and Disease: Molecular and Pharmacological Aspects. *Cells*. 8(7), 728. doi:10.3390/cells8070728
37. Paradies, G., Petrosillo, G., Pistolese, M., Ruggiero, F. M. 2002. Reactive oxygen species affect mitochondrial electron transport complex I activity through oxidative cardiolipin damage. *Gene*. 286(1), 135–141. doi:10.1016/S0378-1119(01)00814-9
38. Pennington, E. R., Funai, K., Brown, D. A., Shaikh, S. R. 2019. The role of cardiolipin concentration and acyl chain composition on mitochondrial inner membrane molecular organization and function. *Biochimica et Biophysica Acta (BBA) – Molecular and Cell Biology of Lipids*. 1864(7), 1039–1052. doi:10.1016/j.bbailip.2019.03.012
39. Petrosillo, G., Portincasa, P., Grattagliano, I., Casanova, G., Matera, M., Ruggiero, F. M., Ferri, D., Paradies, G. 2007. Mitochondrial dysfunction in rat with nonalcoholic fatty liver. *Biochimica et Biophysica Acta (BBA) - Bioenergetics*. 1767(10), 1260–1267. doi:10.1016/j.bbabi.2007.07.011
40. Poljsak, B. 2016. NAD<sup>+</sup> in Cancer Prevention and Treatment: Pros and Cons. *Journal of Clinical & Experimental Oncology*. 5(4), 1–15. doi:10.4172/2324-9110.1000165

41. Rendekova, J., Vlasakova, D., Arsenyan, P., Vasiljeva, J., Nasim, M. J., Witek, K., Dominguez-Alvarez, E., Zeslowska, E., Manikova, D., Tejchman, W., Zaib Saleem, R. S., Rory, K., Handzlik, J., Chovanec, M. 2018. The Selenium-Nitrogen Bond as Basis for Reactive Selenium Species with Pronounced Antimicrobial Activity. *Current Organic Synthesis*. 14(8). doi:10.2174/1570179414666170525104735
42. Robert A. Copeland 2013. *Evaluation of Enzyme Inhibitors in Drug Discovery: A Guide for Medicinal Chemists and Pharmacologists* 2nd edn. John Wiley & Sons, Inc. doi:10.1002/9781118540398
43. Rodriguez, M. E., Azizuddin, K., Zhang, P., Chiu, S. mao, Lam, M., Kenney, M. E., Burda, C., Oleinick, N. L. 2008. Targeting of mitochondria by 10-N-alkyl acridine orange analogues: Role of alkyl chain length in determining cellular uptake and localization. *Mitochondrion*. 8(3), 237–246. doi:10.1016/j.mito.2008.04.003
44. Santo-Domingo, J., Demaurex, N. 2012. The renaissance of mitochondrial pH. *Journal of General Physiology*. 139(6), 415–423. doi:10.1085/jgp.201110767
45. Srivastava, D., Nandi, S., Dey, M. 2019. Mechanistic and Structural Insights into Cysteine-Mediated Inhibition of Pyruvate Kinase Muscle Isoform 2. *Biochemistry*. 58(35), 3669–3682. doi:10.1021/acs.biochem.9b00349
46. Upadhyay, M., Samal, J., Kandpal, M., Singh, O. V., Vivekanandan, P. 2013. The Warburg effect: Insights from the past decade. *Pharmacology and Therapeutics*. 137(3), 318–330. doi:10.1016/j.pharmthera.2012.11.003
47. Wang, P., Sun, C., Zhu, T., Xu, Y. 2015. Structural insight into mechanisms for dynamic regulation of PKM2. *Protein and Cell*. 6(4), 275–287. doi:10.1007/s13238-015-0132-x
48. Warner, S. L., Carpenter, K. J., Bearss, D. J. 2014. Activators of PKM2 in cancer metabolism. *Future Medicinal Chemistry*. 6(10), 1167–1178. doi:10.4155/fmc.14.70
49. Weinberg, F., Hamanaka, R., Wheaton, W. W., Weinberg, S., Joseph, J., Lopez, M., Kalyanaraman, B., Mutlu, G. M., Budinger, G. R. S., Chandel, N. S. 2010. Mitochondrial metabolism and ROS generation are essential for Kras-mediated tumorigenicity. *Proceedings of the National Academy of Sciences of the United States of America*. 107(19), 8788–8793. doi:10.1073/pnas.1003428107
50. Weinberg, S. E., Chandel, N. S. 2015. Targeting mitochondria metabolism for cancer therapy. *Nature Chemical Biology*. 11(1), 9–15. doi:10.1038/nchembio.1712
51. Witek, K., Nasim, M., Bischoff, M., Gaupp, R., Arsenyan, P., Vasiljeva, J., Marć, M., Olejarz, A., Latacz, G., Kieć-Kononowicz, K., Handzlik, J., Jacob, C. 2017. Selenazolinium Salts as “Small Molecule Catalysts” with High Potency against ESKAPE Bacterial Pathogens. *Molecules*. 22(12), 2174. doi:10.3390/molecules22122174

52. Zahra, K., Dey, T., Ashish, Mishra, S. P., Pandey, U. 2020. Pyruvate Kinase M2 and Cancer: The Role of PKM2 in Promoting Tumorigenesis. *Frontiers in Oncology*. 10, 159. doi:10.3389/fonc.2020.00159
53. Zhu, Y., Liu, J., Park, J., Rai, P., Zhai, R. G. 2019. Subcellular compartmentalization of NAD<sup>+</sup> and its role in cancer: A sereNAde of metabolic melodies. *Pharmacology and Therapeutics*. 200, 27–41. doi:10.1016/j.pharmthera.2019.04.002
54. Zichri, S. B., Kolusheva, S., Shames, A. I., Schneiderman, E. A., Poggio, J. L., Stein, D. E., Doubijensky, E., Levy, D., Orynbayeva, Z., Jelinek, R. 2021. Mitochondria membrane transformations in colon and prostate cancer and their biological implications. *Biochimica et Biophysica Acta (BBA) – Biomembranes*. 1863(1), 183471. doi:10.1016/j.bbamem.2020.183471
55. Zu, X. L., Guppy, M. 2004. Cancer metabolism: Facts, fantasy, and fiction. *Biochemical and Biophysical Research Communications*. 313(3), 459–465. doi:10.1016/j.bbrc.2003.11.136

## Acknowledgements

I would like to express my sincerest gratitude to my scientific supervisor and teacher Dr. Pavels Arsenjans for the patience and invested time, who literally stood behind me, sharing knowledge and giving many advice. Thanks to him, I was able to get the best learning and training experience I could even imagine. I will never forget his fantastical master classes and “classical” methods.

I wish to thank my colleagues Alla Petrenko and Dr. Sindija Lapcinska for their helpful contributions and sharing useful chemical insights. Special thanks to prof. Maija Dambrova, Dr. Marina Makrecka-Kuka, Dr. Edijs Vavers, Dr. Baiba Svalbe, Dr. Ilona Domracheva, Ludmila Jackevica, Stanislava Korzh, and the upcoming PhD Melita Ozola for valuable lessons and practical assistance in numerous experiments.

A warm thank you to Dr. Sergey Belyakov for carrying out X-ray analysis and Dr. Kaspars Leduskrasts for the help with the characterisation of luminescence properties.

I am also grateful to Dr. Teodors Pantelejevs for PKM2 expression and for the aid with biophysical experiments, Dr. Marko Hyvonen and Dr. Agnieszka Bogucka for the mass photometry measurements and kind feedback.

I am deeply indebted to my beautiful wife Anna, who listened to my presentations countless times and helped make them understandable to a normal human being.

The completion of my Thesis would not have been possible without the love and unwavering support from my family and friends, and I truly appreciate the care.

I would like to acknowledge the financial support from Latvian Institute of Organic Synthesis (student internal grant IG-2020-01), ERDF “Development of a novel potent PARP inhibitor” (No.1.1.1.1/19/A/016) and BioMedPharm (No. VPP-EM-BIOMEDICINA-2022/1-0001) projects.